



Propagating Neotethys slab break-off beneath Iran following Arabia-Eurasia collision

Annique van der Boon^{a,*}, Marjolein N. Naudé^b, Sara Callegaro^a, Iman Monsef^c, Mahnaz Rezaeian^c, Ali Niknam^c, Laura J. Cotton^d, Petrus le Roux^e, Leo M. Kriegsman^{b,f}, Paul R.D. Mason^b, Cor G. Langereis^b

^a Centre for Planetary Habitability, University of Oslo, P.O. Box 1028, Blindern, NO-0315 Oslo, Norway

^b Department of Earth Sciences, Utrecht University, Princetonlaan 8a, 3584 CB Utrecht, the Netherlands

^c Department of Earth Sciences, Institute for Advanced Studies in Basic Sciences (IASBS), Zanjan 45137-66731, Iran

^d Natural History Museum of Denmark, Universitetsparken 15, 2100 København Ø, Denmark

^e Department of Geological Sciences, University Avenue, Upper Campus, University of Cape Town, Rondebosch 7701, South Africa

^f Naturalis Biodiversity Center, Darwinweg 2, 2333 CR Leiden, the Netherlands

ARTICLE INFO

Keywords:

Adakite
Neotethys arc
Paleogene
Magmatism
Arabia-Eurasia collision
Slab break-off

ABSTRACT

The closure of the Paleo- and Neotethys resulted in a long history of subduction of oceanic crust and production of a large variety of Phanerozoic magmatic rocks in the region occupied by present day Iran. Adakitic rocks of varying ages are common in this area and have distinctive geochemical signatures that have been variably linked to slab break-off or melting of the lower continental crust. The geographic distribution and age of the adakitic rocks indicates a potential younging trend from northwest to southeast Iran, but this trend was interrupted by an older outlier in the area of Tafresh, in the central part of the Neotethys arc. We obtained new geochemical and U-Pb geochronological data for Eocene volcanic and Miocene intrusive rocks from this anomalous locality. Our results show that adakitic signatures are only present in younger Miocene intrusive porphyritic bodies and not in the main calc-alkaline Eocene volcanic succession as previously thought. The Tafresh adakitic porphyritic bodies have an age of 15.7 ± 0.1 Ma ($n = 183$, 2σ SE), which fits well with a regional younging of the adakites towards the southeast of Iran. The Tafresh adakitic rocks are classified as the high-silica variety, and show trace element signatures and isotopic values that are consistent with melting of the lower continental crust. We hypothesise that progressive slab break-off provided a mechanism for the formation of high-silica adakitic rocks along the former Neotethys arc.

1. Introduction

Paleogene magmatic rocks occur in abundance across the area of present-day Iran (Fig. 1A). Calc-alkaline rocks were produced along the Neotethys arc because of the subduction of the Neotethys (Verdel et al., 2011) and the subsequent collision of Arabia with Eurasia during the Paleogene to Neogene (McQuarrie and van Hinsbergen, 2013). Extrusive igneous activity was dominated by an Eocene volcanic flare-up (Verdel et al., 2011), which reached a climax at approximately 40 Ma (van der Boon et al., 2021). Eocene volcanic rocks in the former Neotethys arc generally show continental arc geochemical signatures (Asiabanha and Foden, 2012; Chiu et al., 2013; van der Boon et al., 2017; Verdel et al., 2011), while Miocene and younger rocks in northwest Iran show a shift

towards adakitic compositions (e.g. Shahbazi et al., 2021) and have been interpreted to have formed in a post-collisional setting (e.g. Moghadam et al., 2014). The differing geochemical signatures and ages of these magmatic rocks can be used to trace changes in geodynamic setting, which in turn can be used to constrain the timing of the end of Neotethys subduction and initiation of the Arabia-Eurasia collision. As adakites are often linked to slab break-off (Castillo, 2012), they can provide insight in the timing of geodynamic events in subduction zones.

Adakites are similar in major element composition to calc-alkaline rocks from arc settings, but show a distinctive trace element geochemistry with, amongst other parameters, higher Sr/Y and La/Yb and correspondingly lower Y and Yb (Castillo, 2012). They are typically interpreted to represent partial melting of hot young oceanic basalt in a

* Corresponding author.

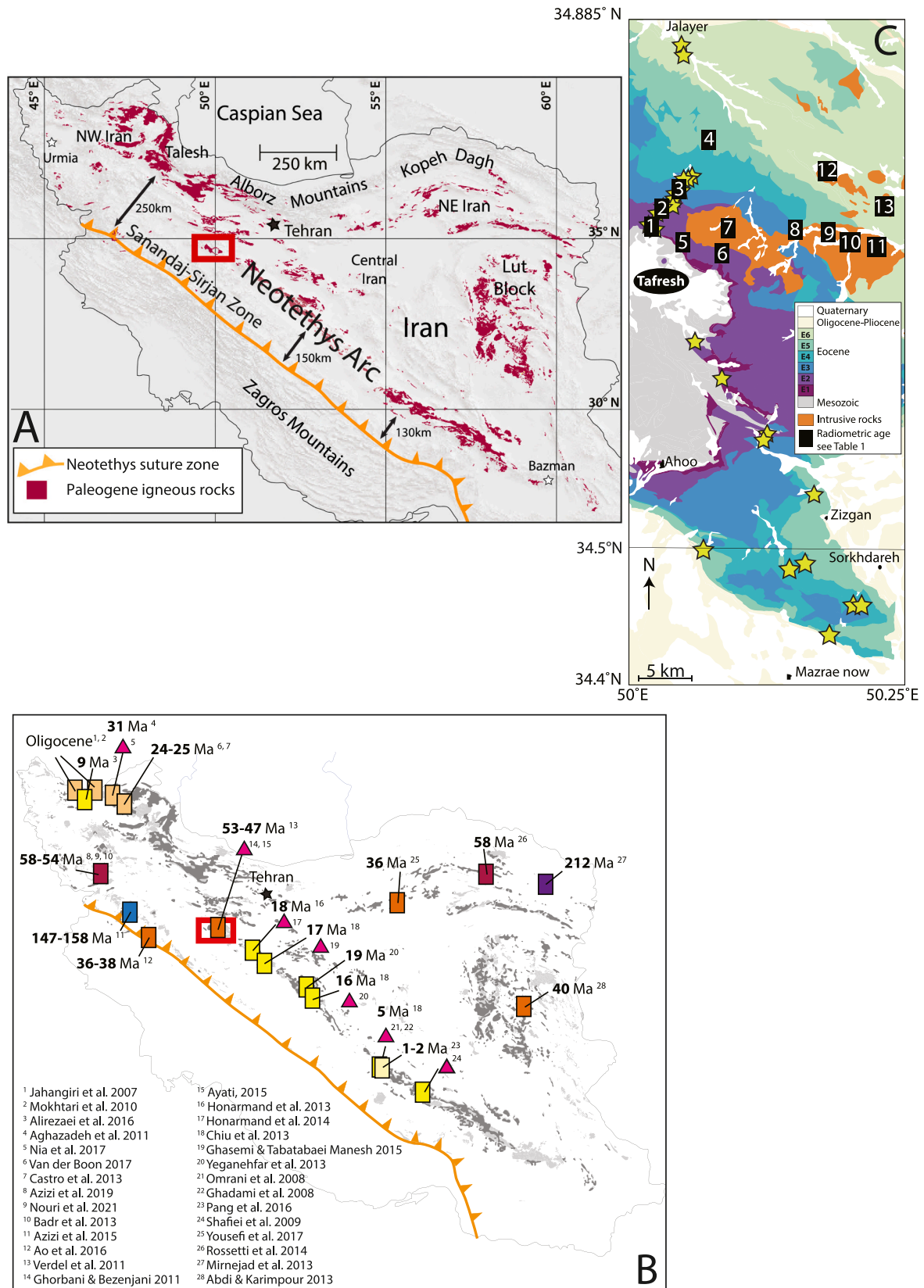
E-mail addresses: avanderboon.work@gmail.com, a.van.der.boon@geo.uio.no (A. van der Boon).

<https://doi.org/10.1016/j.lithos.2024.107737>

Received 27 January 2024; Received in revised form 22 July 2024; Accepted 22 July 2024

Available online 26 July 2024

0024-4937/© 2024 The Authors. Published by Elsevier B.V. This is an open access article under the CC BY-NC-ND license (<http://creativecommons.org/licenses/by-nc-nd/4.0/>).



(caption on next page)

Fig. 1. (A). Map of Paleogene volcanic rocks in Iran (based on Sahandi et al., 2014), and measured distances between the Neotethys arc and the trench (modified after van der Boon et al., 2021). (B). Map showing the spatial and temporal variation of adakitic signatures reported from Iran (Abdi and Karimpour, 2013; Aghazadeh et al., 2011; Alirezaei et al., 2016; Ao et al., 2016; Ayati, 2015; Azizi et al., 2015; Azizi et al., 2019; Badr et al., 2013; Castro et al., 2013; Chiu et al., 2013; Ghadami et al., 2008; Ghasemi and Tabatabaei Manesh, 2015; Ghorbani and Bezenjani, 2011; Honarmand et al., 2013; Honarmand et al., 2014; Jahangiri, 2007; Mirnejad et al., 2013; Mokhtari et al., 2010; Nia et al., 2017; Nouri et al., 2021; Omrani et al., 2008; Pang et al., 2016; Rossetti et al., 2014; Shafiei et al., 2009; van der Boon, 2017; Verdel et al., 2011; Yeganehfar et al., 2013; Yousefi et al., 2017). Pink triangles indicate studies that report geochemistry without radiometric ages. C. Geologic map of the study area with sampling sites (stars) and locations of radiometric ages obtained in previous studies (see Table 1). The northern part, north of latitude 34.5° N is modified after the 1:100,000 scale map of Tafresh (Hadjian et al., 1970), while the map south of latitude 34.5° N is modified after the 1:100,000 scale map of Salafchegan-Khorhe (Alai Mahabadi et al., 2000). (For interpretation of the references to colour in this figure legend, the reader is referred to the web version of this article.)

subducting slab environment (Castillo, 2012; Defant and Drummond, 1990). However, magmas with identical geochemical signatures can also be produced without slab melting, in which case they are termed ‘adakitic’ (Castillo, 2012). Additional mechanisms to produce adakitic compositions include mixing between mafic magma and the evolved products of high-pressure fractional crystallization of arc basalt (Petroni and Ferrari, 2008), as well as partial melting of thickened, eclogitized and delaminated lower crust (Kay and Mahlburg Kay, 1993). In Iran, adakitic magmas have been variably linked to melting of a subducting slab (e.g. Ghorbani and Bezenjani, 2011; Omrani et al., 2008), as well as melting of the lower crust (Kheirikhah et al., 2020; Pang et al., 2016; Torkian et al., 2019). Determining the timing of adakite formation in Iran could provide maximum age constraints on the collision of Arabia and Eurasia, provided that the adakites were generated through slab break-off after collision. Most adakitic rocks found along the former Neotethys arc are of Oligocene-Miocene age and show a progressing age trend from the oldest adakites in NW Iran towards younger adakites in the southeast (see Fig. 1B). They range in age from Early Oligocene (30.8 Ma; Aghazadeh et al., 2011) to Pleistocene (1.15 Ma; Pang et al., 2016) in the southeast. However, near Tafresh, a city ~150 km south-west of Tehran, Ghorbani and Bezenjani (2011) reported the presence of adakitic rocks of Eocene age, which form an outlier to this trend. Ghorbani and Bezenjani (2011) did not provide radiometric ages or sample locations for the adakitic rocks, but volcanic rocks in the vicinity were dated by Verdel et al. (2011) at an age of 52.9 Ma (early Eocene). Verdel et al. (2011), however, provide no geochemical data for the dated samples, but report the geochemistry of some other volcanic rocks in this area, without finding any evidence for adakitic signatures. Another study was performed by Ghorbani et al. (2014), who provided K/Ar ages for volcanic rocks that show Oligocene-Miocene ages for the volcanic succession. These ages are around 30 million years younger than the U-Pb zircon and Ar-Ar ages obtained by Verdel et al. (2011), and also conflict the biostratigraphic constraints from larger benthic foraminifera (Flandrin and Hadjian, 1970) that constrained the succession to an Eocene age.

In addition to the anomalous geochemical signatures, a conspicuous change occurs in the geometry of the Neotethys arc around Tafresh. Presently, the main Zagros thrust is regarded as the suture between Arabia and Eurasia (Agard et al., 2011; see Fig. 1), and is assumed to be the location of the former Neotethys trench (e.g. Shafaii Moghadam et al., 2020). Near Tafresh, the distance between the Neotethys arc and the suture zone changes from ~20 km to ~150 km (Fig. 1A). This led van der Boon (2017) to hypothesise that subduction of a flatter slab under the western Alborz led to a slab-tear beneath the Tafresh region, which could explain both the Eocene adakites and the larger arc-trench distance in the Talesh and western Alborz Mountains.

In this study, we investigated volcanic and intrusive rocks in the Tafresh region to elucidate their geochemical signature and emplacement age. Our sampling was focused on Eocene volcanic rocks and intrusive rocks that crosscut the volcanic succession. We present new whole-rock major and trace element geochemistry, as well as Sr-Nd-Pb isotopes and zircon U-Pb geochronology. We aim to determine which rocks show adakitic signatures and date the adakitic rocks more accurately to constrain the tectonic setting in the Tafresh region. We then reassess the potential time progression seen in adakitic magmatism

along the Neotethys arc. Our study is the first to report radiometric ages and adakitic signatures from the same rocks. We now show that the Eocene volcanic rocks do not exhibit adakitic signatures, and that the adakitic signatures are found only in intrusive rocks that formed during the Miocene. This means that the adakitic rocks around Tafresh no longer form an outlier in the age progression trend.

2. Geological setting

The Mesozoic to Cenozoic geology of Iran was shaped by the opening and closure of the Paleotethys and Neotethys along rifts and subduction zones, the latter of which resulted in large-scale arc magmatism. The remnants of magmatic arcs are found in discrete belts and blocks across present-day Iran (Fig. 1A), which is made up of several tectonic blocks that drifted away from Gondwanaland during the closure of the Paleotethys (the so-called ‘Cimmerian’ blocks). During the Mesozoic, the Neotethys closed along a subduction zone that produced magmatism in the Sanandaj-Sirjan Zone (SSZ; Fig. 1), which started during the Triassic and culminated in the Jurassic. From the Cretaceous to the Eocene, magmatism along the SSZ ceased and the volcanic arc shifted towards a more northerly position. Magmatism continued in this northerly belt during the Cenozoic, with a peak of activity during the middle Eocene (ca. 40 Ma; Chiu et al., 2013; van der Boon et al., 2021; Verdel et al., 2011). This belt, which was the main Neotethys arc during the Paleogene, runs from the northwest of Iran towards the southeast. Geochemical signatures of magmatic products in this Neotethys arc are indicative of a continental arc setting (Asiabanha and Foden, 2012; Verdel et al., 2011). Arc volcanism in this belt ended after the Neotethys had closed, because of the collision of Arabia and Eurasia (McQuarrie and van Hinsbergen, 2013). After collision, the Neotethys slab broke off (Omrani et al., 2008), which resulted in renewed magmatic activity in this belt, but with different geochemical signatures. The exact timing of the Arabia-Eurasia collision is widely debated, with the date of the onset ranging from as early as the Late Cretaceous to middle Miocene-Pliocene (see overview in McQuarrie and van Hinsbergen, 2013). The Arabia-Eurasia collision is generally regarded as diachronous (Darin and Umhoefer, 2022), with the NW of Iran undergoing the earliest collision as well as the earliest changes in volcanic regime and geochemical affinity. Miocene post-collisional volcanism in NW Iran shows signatures characteristic of a subduction-modified subcontinental lithospheric mantle (Moghadam et al., 2014), while Quaternary volcanic rocks show an increased influence of asthenospheric upwelling, leading to more ocean island basalt (OIB)-like geochemical signatures (Ghalamghash et al., 2019). Subduction-related magmatism continued well into the Miocene for the south-eastern part of the Neotethys arc (Chiu et al., 2013).

2.1. Cenozoic geology of the Tafresh region

2.1.1. Description

The geology around Tafresh is dominated by Eocene volcanic rocks (Fig. 1C). Hadjian et al. (1970) distinguished Eocene units E1 to E6 around Tafresh, with a cumulative thickness of the entire Eocene succession around 3000 m (a detailed geologic map, as well as a full legend of maps is provided in Supplementary Files S1 and S2, respectively). A

conspicuous feature is the Tafresh caldera, to which the Eocene volcanic succession is related (Ghorbani and Bezenjani, 2011). Unit E1 overlies Cretaceous sediments, and consists only of sedimentary rocks, and was thus not sampled in our study. The lower part of E1 consists of basal red beds, indicating terrestrial conditions. Depositional environments throughout the remainder of the succession are predominantly shallow marine (based on the abundant presence of *Nummulites*, larger benthic foraminifera), sometimes interrupted locally by terrestrial settings. Unit E1 marks a return of marine conditions to an area that was previously subaerially exposed. Unit E1 contains conglomerates with clasts of Cretaceous and Jurassic rocks (Flandrin and Hadjian, 1970). Hadjian et al. (1970) reported an Ypresian age (56–47.8 Ma) for E1, based on larger benthic foraminifera. Unit E2, for which a Lutetian (47.8–41.2 Ma) age is inferred, consists of mostly felsic ignimbrites intercalated with minor nummulitic limestones. Unit E3 consists mostly of sedimentary rocks, and contains two sub-units, one with trachyandesitic lava flows, the other one made up of nummulitic limestones. Unit E4 consists of tuffaceous beds intercalated with limestone and rhyolitic lavas, and includes two sub-units, one consisting of rhyolite and one consisting of nummulitic limestones. Within the bounds of the Tafresh map, unit E5 consists mainly of sedimentary rocks with some rhyolitic lavas and tuffs, and no outcrops of igneous rocks are located along our sampled profile (Fig. 1C). The unit is assigned a Lutetian age and has one sub-unit of nummulitic limestones. Unit E6 is made up mostly of pyroclastic beds, with intercalations of andesitic lava, nummulitic limestones and gypsum. Several sub-units of nummulitic limestones and gypsum are defined. Hadjian et al. (1970) reported the occurrence of *Nummulites fabianii*, which indicates a Priabonian (37.7–33.9 Ma) age (Agnini et al., 2011) for unit E6. More detailed descriptions of these units including lithological logs are given in Flandrin and Hadjian (1970).

Overall, the Eocene succession records a shallow marine environment with repeated evidence of explosive volcanism, which was enhanced by the interaction of magmas with seawater upon eruption (Hadjian et al., 1970). The Eocene succession is overlain by an angular unconformity with red conglomerates of the Lower Red Formation of Oligocene age (Hadjian et al., 1970). The red conglomerates indicate a shift towards prolonged continental conditions, with sediments sourced from an emerged area south of Tafresh (Hadjian et al., 1970). Minor volcanism continued during the Oligocene, with some basaltic lava flows north of our sampled area. During the late Oligocene, marine conditions returned for a final time, as recorded by the Oligo-Miocene Qom Formation limestones (~27–18 Ma). On top of the Qom formation, extensive continental sediments of the Upper Red Formation were deposited, with volcanism of the same age. Volcanism in the Miocene-Pliocene is more voluminous than during the Oligocene, but much less

voluminous than in the Eocene (based on geological maps and cross-sections). The geological map of Tafresh shows two sets of dykes that crosscut the rocks in the area around Tafresh, one set is believed to be related to Eocene volcanism, while the other set is related to Miocene-Pliocene volcanism (Fig. S1). Dykes that are mapped as Eocene crosscut the Eocene succession, while the Miocene-Pliocene dykes mostly crosscut Miocene volcanic rocks and Oligocene-Miocene sedimentary rocks. The younger set of dykes has been interpreted to have formed in response to wrench tectonics (Emami, 1981). During the early Miocene (~20 Ma), several plutonic bodies were emplaced in the Eocene volcanic succession around Tafresh (Mirnejad et al., 2019).

2.1.2. Ages

Several studies have reported radiometric ages of units along the road north of Tafresh. We report locations of dated samples in Fig. 1C and ages in Table 1. Verdel et al. (2011) obtained Eocene ages (Ypresian-Lutetian) on the basis of U-Pb and Ar/Ar radiometric dating for volcanic rocks from units E2, E3 and E4. However, Ghorbani et al. (2014) reported Oligocene-Miocene ages for volcanic rocks of units E2 and E4, based on K/Ar dating of two lavas in unit E2 and a dike or sill in unit E4. Oligocene-Miocene ages contrast the ages obtained by Verdel et al. (2011), as well as the general assessment of biostratigraphy based on abundant *Nummulites* in volcanoclastic rocks of units E2-E6. Intrusive rocks were dated as Miocene (~20 Ma) by Mirnejad et al. (2019). Intrusions further to the east of the studied area were also dated as Miocene (~21 Ma) by Raeisi et al. (2020). Chaharlang and Ghorbani (2020) provide Miocene ages for dykes that crosscut the Eocene units, which could indicate that at least some of the dykes mapped as Eocene are in fact of Miocene age.

2.2. Field relations

We sampled volcanic rocks and dykes, as well as plutonic bodies that crosscut the volcanic succession. Representative outcrop pictures are presented in Fig. 2. We sampled rocks in two localities, one to the north of Tafresh ('North Tafresh') and the other to the southeast of Tafresh ('Southeast Tafresh'). We refer to the geographic locations where samples were taken as 'sites', while 'samples' refer to individual rock samples. Samples with prefix MT were taken from the North Tafresh locality, along the road from Tafresh to Jalayer (Fig. 1C). Samples with prefix MS were taken at the Southeast Tafresh locality, along a road going from Tafresh to Zizgan, as well as along two roads that are more to the southeast from Zizgan to Hezar Abad and Sorghdareh to Mazrae Now (Fig. 1C; S1). An overview of samples and their respective units is presented in Supplementary File S3.

Table 1

Overview of previously published radiometric ages from units in Fig. 1C (Babazadeh et al., 2022; Chaharlang and Ghorbani, 2020; Ghorbani et al., 2014; Mirnejad et al., 2019; Verdel et al., 2011). Numbers correspond to the numbers on Fig. 1C. n/g = not given in the original paper, * indicates that this is a crosscutting relationship to the mentioned unit.

Unit	Rock type	Sample	Age	Uncertainty	Epoch	Age	Method	Study	Number
E ₂	Green tuff	TF4a	56.61	1.93	Paleocene	Thanetian	Ar/Ar	Verdel et al., 2011	1
E ₂ ^g	Andesite flow	TF3	54.7	3.1	Eocene	Ypresian	U-Pb	Verdel et al., 2011	1
E ₂	Volcanic	TF6	52.9	3.3	Eocene	Ypresian	U-Pb	Verdel et al., 2011	2
*E ₂	Dike	TA17	21.23	n/g	Miocene	Langhian	U-Pb	Chaharlang and Ghorbani, 2020	2
E ₃	Volcanic	TF7a	47.4	1.7	Eocene	Lutetian	U-Pb	Verdel et al., 2011	3
E ₄	Volcanic	TF11	44.3	2.2	Eocene	Lutetian	U-Pb	Verdel et al., 2011	4
*E ₄	Dyke, sill	TF5	15.4	0.9	Miocene	Langhian	K/Ar	Ghorbani et al., 2014	4
E ₂	Lava	TF9	26	1.6	Oligocene	Chattian	K/Ar	Ghorbani et al., 2014	5
E ₂	Lava	TF2	26.8	10.8	Oligocene	Chattian	K/Ar	Ghorbani et al., 2014	6
g	Granitoid	SG13	19.07	0.25	Miocene	Burdigalian	U-Pb	Mirnejad et al., 2019	7
g	Granitoid	AH5	20.37	0.41	Miocene	Burdigalian	U-Pb	Mirnejad et al., 2019	8
g	Granitoid	KA2	20.27	0.42	Miocene	Burdigalian	U-Pb	Mirnejad et al., 2019	9
g	Granitoid	NG1	19.47	0.16	Miocene	Burdigalian	U-Pb	Mirnejad et al., 2019	10
g	Granitoid	GN1	20.19	0.39	Miocene	Burdigalian	U-Pb	Mirnejad et al., 2019	11
g	Granitoid	TF9	22.4	0.7	Miocene	Aquitania	U-Pb	Babazadeh et al., 2022	12
g	Granitoid	TF12	22.7	0.5	Miocene	Aquitania	U-Pb	Babazadeh et al., 2022	13

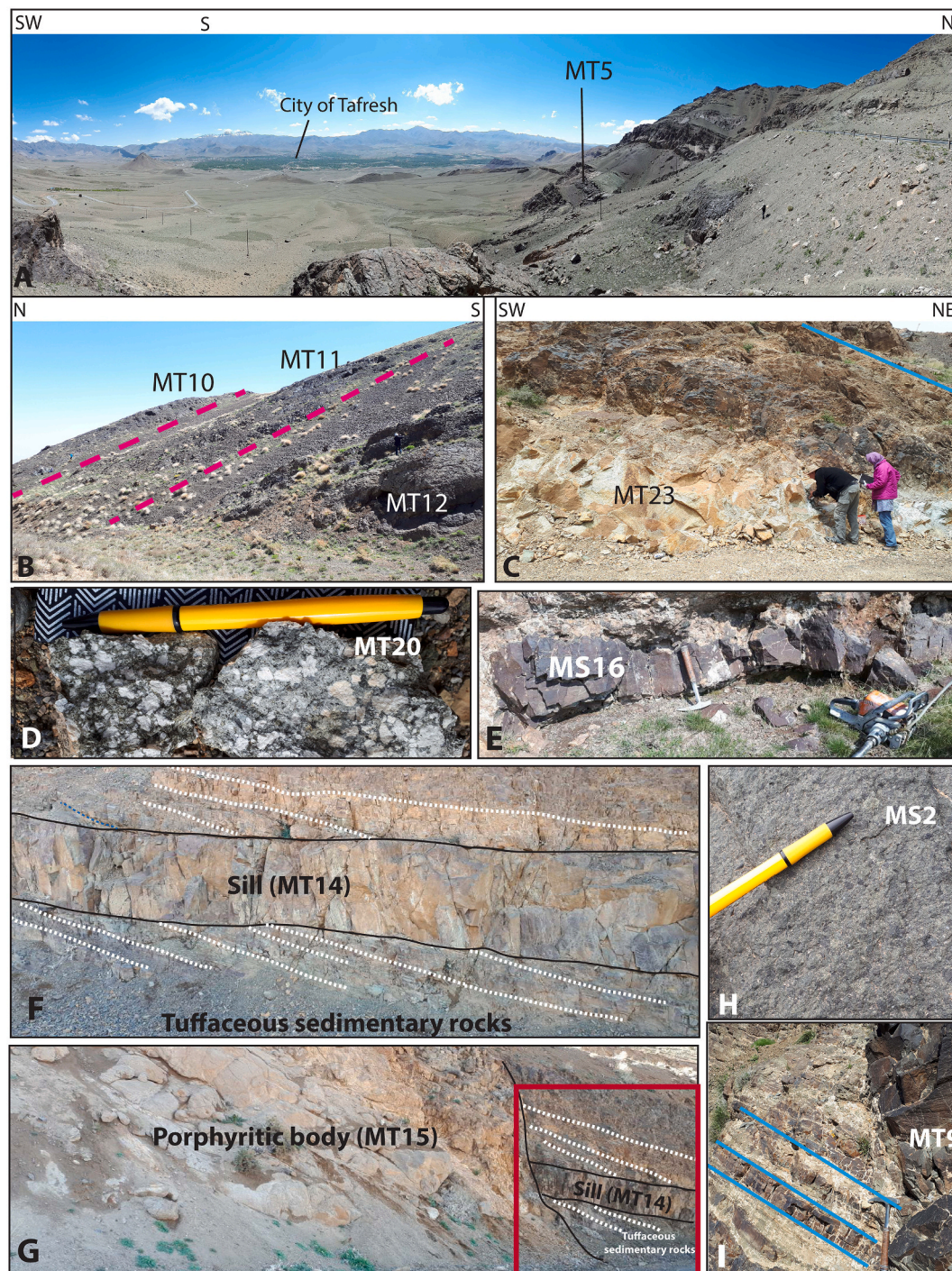


Fig. 2. Images of some of the sampled field sites. (A). Panoramic view into the Tafresh caldera (looking towards the SE) with the northern flank of the caldera on the right side of the picture. (B). Succession of lava flows of sampled sites MT10–12, pink dotted lines indicate bedding attitudes. (C). Porphyritic body MT23 intruded into sedimentary rocks, the blue line indicates the bedding of the sedimentary rocks. (D). Coarse grained porphyritic body MT20. (E). Dacitic lava MS16. (F). Sill MT14 intruded into tuffaceous sedimentary rocks. (G). Structural relations between sites MT14 and MT15, red square corresponds to Fig. 2F. MT14 is a fine-grained sill that crosscuts Eocene tuffaceous sedimentary rocks at a small angle, and is likely part of the Eocene succession. MT15 is a coarse-grained porphyritic body that crosscuts both the sedimentary rocks and the sill. (H). Trachybasaltic lava MS2. (I.) MT9 is a dyke that crosscuts sedimentary rocks (bedding of the sedimentary rocks indicated by blue lines). (For interpretation of the references to colour in this figure legend, the reader is referred to the web version of this article.)

2.3. North Tafresh locality

Most samples along this profile were taken in unit E2, with additional samples from units E3, E4 and E6. The start of the North Tafresh profile is in the E2 unit, where there are three distinct lava flows interbedded with a succession of tuffaceous siltstones. The flows consist of rhyolitic

lavas (MT1 and MT3) and pillow lavas (MT2 and MT4). This part of the succession is capped by a large ignimbrite of approximately 100 m thick, which forms a distinctive bed that runs horizontally across the lower foothills of the surrounding area (MT5). This is the oldest visible part of the Eocene directly north of Tafresh, which unconformably overlies Cretaceous sediments (Fig. 2A). Verdel et al. (2011) dated a green tuff

and an andesite flow in the base of unit E2 using Ar/Ar geochronology on plagioclase and U-Pb dating on zircons at 56.61 ± 1.93 Ma and 54.7 ± 3.1 Ma (late Paleocene-early Eocene), respectively. Continuing upward in the stratigraphy, the ignimbrite is followed by a succession of tuffaceous sediments, shales, pyroclastic rocks and breccia, interbedded with mafic lavas (MT6, MT10–13, MT16–18), and cross-cut by some fine-grained sills and dykes (MT8, MT9), which all belong to unit E2 (Hadjian et al., 1970). Verdel et al. (2011) obtained a U-Pb zircon radiometric age of 52.9 ± 3.3 Ma from a volcanic rock (not further specified) sampled near our sites MT10–13. Sample MT14 comes from a sill that crosscuts tuffaceous sediments (Fig. 2F), and which itself is in turn crosscut by a larger, intrusive, porphyritic body (MT15; Fig. 2G). The porphyritic body contains plagioclase megacrysts and hexagonal biotite in a fine-grained matrix. There are several porphyritic bodies of several meters thick, and some can be traced laterally for a few hundred metres, although they are not mapped on the geologic map of Tafresh. These porphyritic bodies also crosscut units E3 and E4 (MT19–21, MT23–25; see Fig. 2F), and are thus younger than units E3 and E4. Verdel et al. (2011) report a U-Pb zircon age of 47.4 ± 1.7 Ma (middle Eocene) for a volcanic rock (not further specified) of unit E3. Verdel et al. (2011) dated the top of unit E4 at 44.3 ± 2.2 Ma (middle Eocene; U-Pb zircon age). The uppermost samples (MT27–28) from the northern section belong to the E6 unit. The Eocene units are separated from the younger Lower Red Formation by a large thrust fault, which was poorly exposed.

2.4. Southeast Tafresh locality

Samples taken in the Southeast Tafresh locality were collected from units E2, E3, E4 and E5, on the geologic maps of Tafresh (Hadjian et al., 1970) and Salefchegan-Khorhe (Alai Mahabadi et al., 2000). The first site southeast of Tafresh includes a 1.5 m-thick felsic dyke (MS1) of unknown age, crosscutting a grey marl of likely Cretaceous age. Samples MS2–5 were taken from a ~ 100 m thick volcanic unit belonging to E2. Further southeast, an outcrop of unit E4 shows pillow lavas (MS6) in a faulted and sheared unit that is strongly tilted. On top of this, a lava flow crops out (sample MS7, unit E3) and lies conformably above sediments and below a tuff sequence. The latter is topped by a volcanoclastic breccia containing 10 cm to 1 m size clasts of country rock (mainly tuff) and pumice. A fault runs between sites MS6 and MS7. Site MS8 is within unit E5 and consists of a tuff. All other sites are mostly within unit E4, with the exception of MS14, which is in unit E5. In all these sites dacitic and rhyolitic lava flows crop out, occasionally alternated by conformable Eocene limestone beds.

The Southeast Tafresh locality is at much lower altitude compared to the northern profile and contains lavas with a more rhyolitic composition. The Southeast Tafresh locality is structurally more complex, with folds and faults that cut the succession. There are no intrusive porphyritic bodies in the Southeast Tafresh locality that resemble the ones found in the North Tafresh locality.

3. Analytical methods and results

3.1. Petrography and geochemistry

We sampled 38 lava flows, dykes, sills, ignimbrites and tuffs from the main Eocene volcanic succession, as well as 7 porphyritic intrusive bodies that crosscut the volcanic succession. Most samples were collected as drill cores, using standard paleomagnetic sampling techniques (e.g. van der Boon et al., 2017), in order to provide material that was minimally affected by surface weathering. Additionally, several larger hand samples were taken for petrography and radiometric dating.

In the following description of the geochemical results, we group the rocks by their mode of occurrence, i.e. (pillow) lavas, dykes, sills, intrusive rocks, and pyroclastic rocks (ignimbrite and volcanoclastic rocks). Detailed descriptions of all the analytical methods used are given

in Supplementary File S4. Whole-rock major and trace element geochemical data for 38 samples are given in supplementary file S5. Rock samples collected from the E2-E6 volcano-sedimentary sequence were generally affected by hydrothermal alteration. This is reflected by the petrography (see examples in S6), where most sampled rocks contain altered phenocrysts, e.g., sericitized feldspars, and secondary phases such as chlorite and calcite in the groundmass. In the freshest samples, typical textures of supra-subduction zone volcanic rocks are visible, with zoned plagioclase phenocrysts, euhedral amphibole phenocrysts and plagioclase glomerocrysts. Similarly, the subvolcanic rocks (dykes and sills) and the intrusive bodies (Fig. 2C; S6) are visibly altered, with largely sericitized plagioclase phenocrysts and biotite phenocrysts that show substitution by secondary opaque phases. Loss on ignition (LOI) varies between 1.5 and 8 wt% in the analysed samples, with two notable outliers up to 12 wt% (MS9 and MS10; discarded from the plots for suspected analytical problems in the alkali measurements). The presence of carbonates as secondary phases is confirmed by the correlation between LOI and CaO (S7), while Sr, Ba and alkali metal concentrations do not correlate with LOI. Nevertheless, the great scatter shown by alkali metals when plotted vs. SiO₂ or MgO (S8) suggests that they were affected by alteration, and we hence favour classification diagrams based on immobile elements (e.g. Pearce, 1996; Wood, 1980; Fig. 3A, B; but cf. TAS and K₂O vs. SiO₂ in S8 and S9). Eocene lavas show a bimodal character, with a group that classifies as calc-alkaline basalts to andesites (SiO₂ 45.97–57.38 wt%; Zr/Ti 0.55–0.1; MgO 3–9 wt%; Fig. 3A–C), and a more evolved group that classifies as dacites to rhyolites (SiO₂ 68.17–57.38 wt%; Zr/Ti < 0.016; MgO < 1 wt%). The high Al₂O₃ and K₂O and relatively low MgO classifies the Eocene volcanics as a high-K calc-alkaline series, typical of supra-subduction environments (S8). The dykes and sills bridge the gap between the two end-member groups, classifying as andesites to basaltic andesites and plotting along a broadly calc-alkaline differentiation trend on an AFM diagram (Fig. 3C). Of the two pyroclastic rocks for which trace elements were analysed, one (MS8) overlaps with the basaltic group, while the other (MT5; Fig. 3A) overlaps with the evolved group. The three volcanoclastic rocks, for which only major elements are available, plot in-between the two groups, broadly overlapping with the sills and dykes (S8, S9). The intrusive porphyritic bodies stand out from the rest of the samples through their distinctive chemistry. They are classified as trachyandesites in the Pearce (1996) discrimination diagram (Nb/Y ≈ 1, vs. Nb/Y < 0.6 for the other volcanics; Fig. 3A), and as diorites to granodiorites in the intrusive version of the TAS diagram (S9). Volcanic rocks show positive correlations between K₂O and SiO₂ (S8), with the exception of sample MS16, which shows an anomalously low K₂O value. Concentrations of MgO, Fe₂O₃tot, Al₂O₃, Na₂O, and MnO show a negative correlation with SiO₂ (Fig. 3D–G). In these variation diagrams, all samples plot coherently as a rather uniform group, despite some scatter. The intrusive porphyritic samples are in line with the volcanic rocks, with intermediate compositions (SiO₂ 61–64 wt%) and form a cluster. CaO concentrations and trends are not informative due to the presence of secondary carbonates. P₂O₅ and TiO₂ (Fig. 3F,G) show incompatible behaviour for the less evolved group of volcanics meaning that the amount of P₂O₅ and TiO₂ increases together with silica (0.6–1.6 wt% TiO₂; 0.04–0.26 wt% P₂O₅). The dyke sample MS4 belongs to this group. In the dacitic-rhyolitic rocks, TiO₂ and P₂O₅ are relatively low (0.5–1 wt% TiO₂; 0.1–0.19 wt% P₂O₅) and do not correlate with SiO₂. For TiO₂, the same pertains to the sills and the dykes, but with more scatter. The sills are rich in P₂O₅ (>0.25 wt%) compared to the rocks in the rest of the dataset. With respect of the rest of the dataset the porphyritic bodies are poor in TiO₂ (0.46/0.6 wt%) and rich in P₂O₅ (0.18–0.22 wt%).

Rare Earth Elements (REE) were plotted on chondrite-normalised (McDonough and Sun, 1995) diagrams (Fig. 4A–D). The lava samples show variable concentrations of REE, increasing from ca. 20 to 200 times chondrite from basaltic to rhyo-dacitic samples (Fig. 4A,B). All the lavas show relatively flat profiles, with slightly fractionated Light REE (LREE) to Heavy REE (HREE; average La/Yb_N = 1.8) and Middle (MREE)

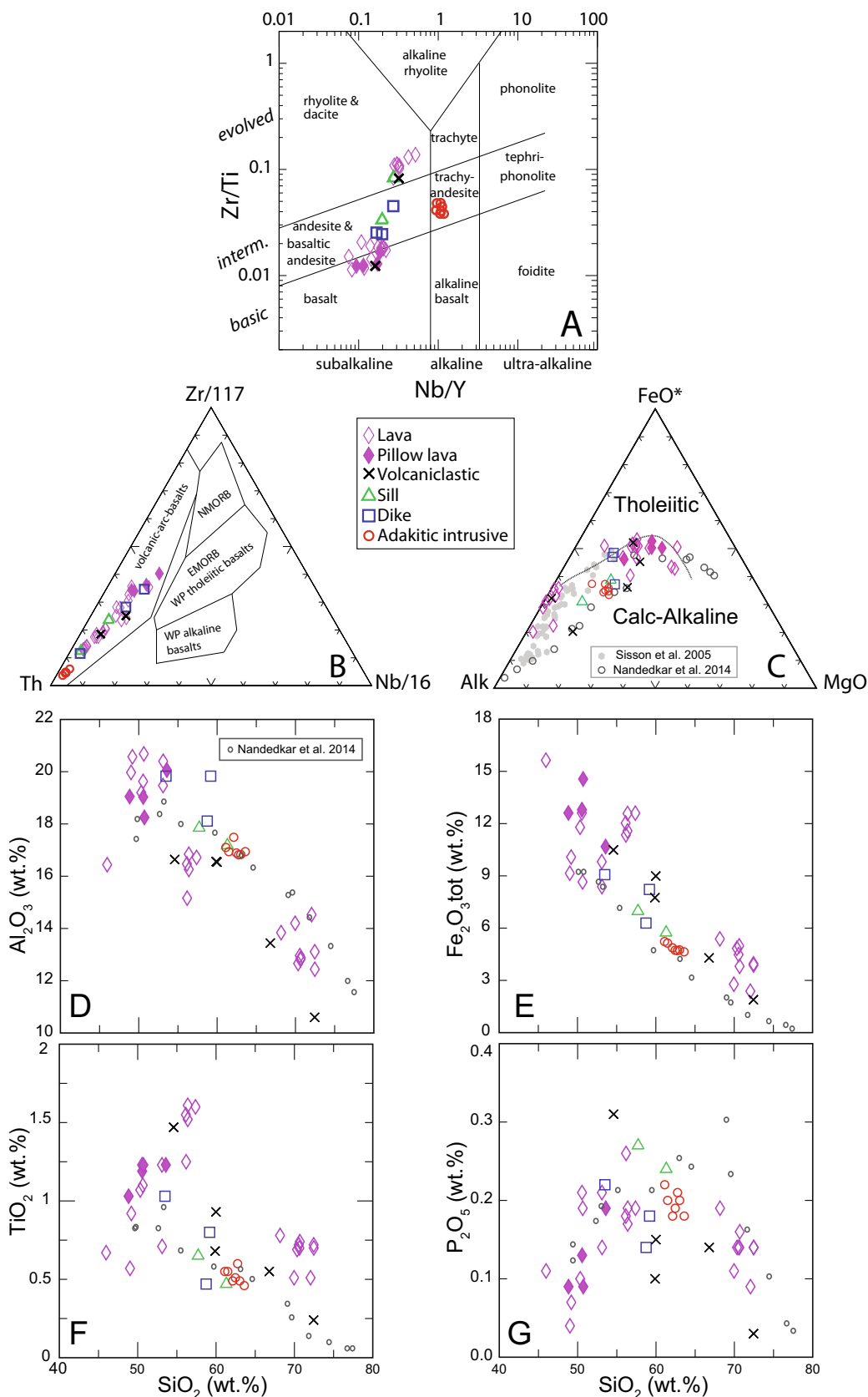


Fig. 3. Classification of samples (LOI < 6%) based on (A). Zr/Ti versus Nb/Y content (Pearce, 1996). (B). Zr, Th, Nb ternary diagram with basalt discriminants of Wood (1980) WP – within plate, NMORB – normal mid-ocean ridge basalt, EMORB – enriched mid-ocean ridge basalt. (C). AFM diagram (Alk = Na₂O + K₂O, F = FeO_{tot}, M = MgO; wt%) discriminates tholeiitic and calc-alkaline magmatic series (Irvine and Baragar, 1971). Data sources and experimental conditions: Sisson et al. (2005): basalt, 1.7–2.3 wt% H₂O, equilibrium crystallization, NNO –1.3 to +4, 0.7 GPa; Nandedkar et al. (2014): basalt, 3 wt% H₂O, fractional crystallization, NNO +0.3 to +1.7, 0.7 GPa. (D-G). major element Harker diagrams of D. Al₂O₃, E. Fe₂O₃, F. TiO₂, G. P₂O₅ versus SiO₂.

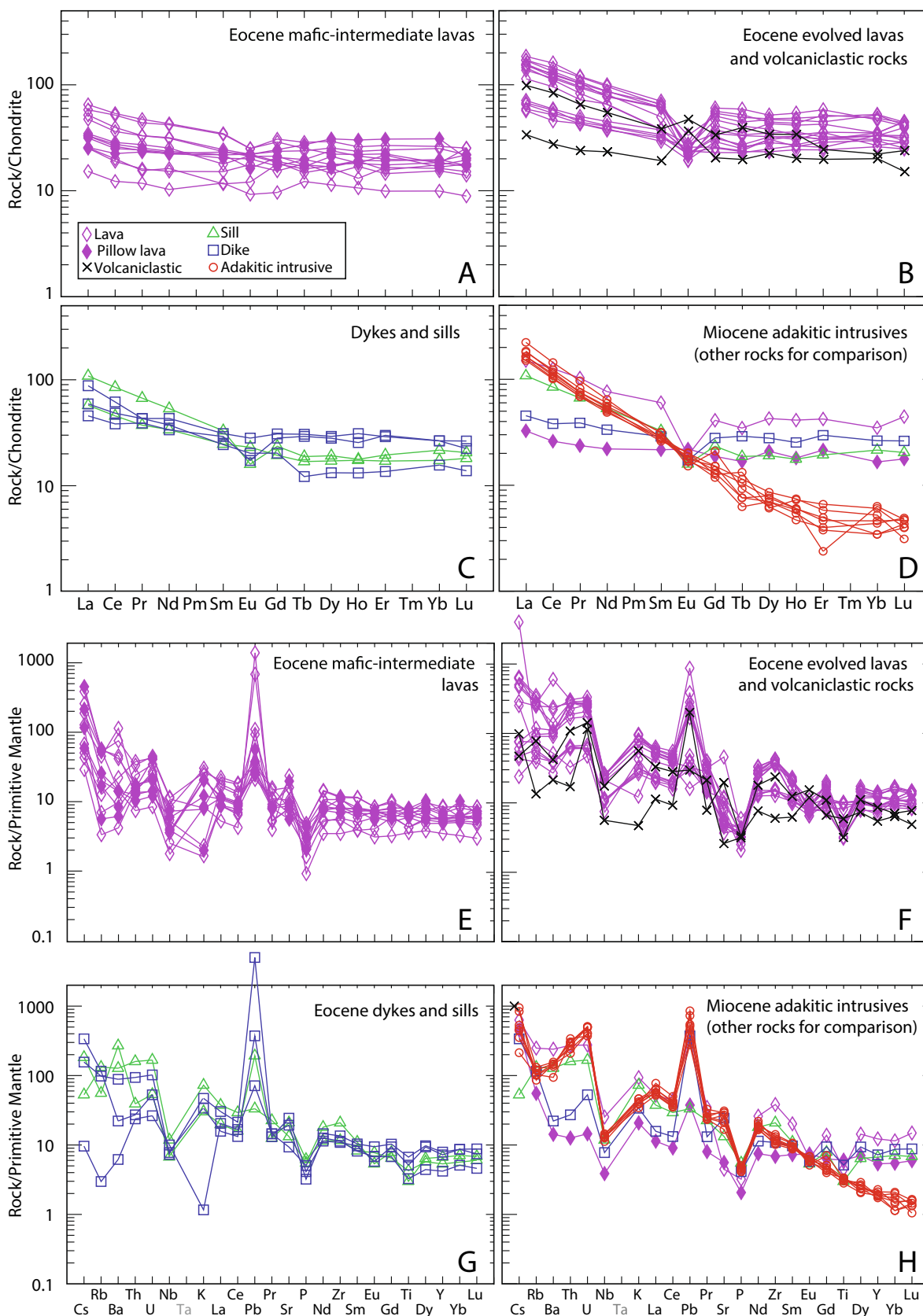


Fig. 4. Chondrite-normalised (McDonough and Sun, 1995) spider diagrams for (A). Eocene mafic to intermediate (pillow) lavas, (B). Eocene evolved lavas (trachyandesites, dacites and rhyolites) and volcaniclastic rocks, (C). Eocene dykes and sills, (D). Miocene adakitic intrusives with other rocks for comparison (dyke MS1, sill MT8, mafic pillow lava MS5 and evolved lava MS13). Primitive mantle-normalised (Sun and McDonough, 1989) spider diagrams for (E). Eocene mafic to intermediate lavas, (F). Eocene evolved lavas and volcaniclastic rocks, (G). Eocene dykes and sills, (H). Miocene adakitic intrusives with same rocks as Fig. 5D for comparison. Ta values are not plotted due to suspected contamination by the W-carbide grinder during sample preparation.

to Heavy REE (average $\text{Sm}/\text{Yb}_N = 1$). The evolved group of lavas show pronounced negative Eu anomalies, and more fractionated LREE/MREE profiles (average $\text{La}/\text{Sm}_N = 2.5$) with respect to the basaltic-andesitic samples (average $\text{La}/\text{Sm}_N = 1.7$), as visible on a plot of La/Sm vs. La (S10). The two volcanoclastic rocks share very similar REE patterns with the Eocene lavas, but with a positive Eu anomaly (Fig. 4B). Because these volcanoclastic rocks might contain a significant fraction of lithic fragments, we discard them from further geochemical discussion. The sills and the dykes share similar REE patterns with moderately evolved lava samples (Fig. 4C). The porphyritic bodies show very different REE patterns, with the highest La concentrations (35–55 ppm, ca. 200 times chondrite; Fig. 4D) and very steep profiles (LREE/HREE average $\text{La}/\text{Yb}_N = 37.8$). They do not show Eu anomalies.

Trace elements were plotted on primitive mantle-normalised (Sun and McDonough, 1989) multielement diagrams (Fig. 4E–H). All samples show strong negative Nb anomalies, which are a classical feature of subduction related magmas. The felsic lava samples, as well as dykes, sills, and volcanoclastic rocks show a negative anomaly in Ti, which is not recorded by mafic lavas and intrusive rocks. All samples except the most evolved lavas show strong positive Pb anomalies. All the rocks show a moderate to strong large-ion lithophile element (LILE)/LREE enrichment, particularly evident in the intrusive samples (Fig. 4H). The latter show the steepest incompatible element patterns, with progressively more depleted MREE towards HREE, likely indicating the presence of residual garnet in the source.

The porphyritic intrusions show a clear adakitic signature according to the criteria of Castillo (2012), by showing high LREE/HREE (La/Yb 40–70), high Sr/Y (45–75) accompanied by low Y (<10 ppm; Fig. 5). This signature is not shown by the Tafresh volcanic rocks.

Whole-rock Sr-Nd-Pb isotopic data for 20 selected samples are given in Supplementary File S11. Initial isotopic values were calculated using an average age of 40 Ma (~peak of the magmatic flare-up; van der Boon et al., 2021) for volcanic rocks, and 15.7 Ma for porphyritic bodies. Choosing different ages within this relatively limited age range for the analysed samples does not significantly change the isotope ratios. The Tafresh Eocene volcanics and the single analysed dyke sample range in $^{87}\text{Sr}/^{86}\text{Sr}_{40\text{Ma}}$ from 0.705491 to 0.707773, and in $^{143}\text{Nd}/^{144}\text{Nd}_{40\text{Ma}}$ ($\epsilon\text{Nd}_{40\text{Ma}}$) from 0.512524 (–1.23) to 0.512752 (+3.22) (Fig. 6A). The analysed sills plot on the more depleted side of the range, with $^{87}\text{Sr}/^{86}\text{Sr}_{40\text{Ma}}$ from 0.705768 to 0.705815, and in $^{143}\text{Nd}/^{144}\text{Nd}_{40\text{Ma}}$ ($\epsilon\text{Nd}_{40\text{Ma}}$) from 0.512694 (–2.09) to 0.512657 (+1.38). The porphyritic intrusives with adakitic signature plot as a tight cluster centred at ca.

$^{87}\text{Sr}/^{86}\text{Sr}_{15.7\text{Ma}}$ 0.7066 and $^{143}\text{Nd}/^{144}\text{Nd}_{15.7\text{Ma}}$ 0.51255 (–1.2). The isotopically most depleted samples plot close to the Bulk Silicate Earth value (BSE; Zindler and Hart, 1986) and the more enriched ones trend towards more radiogenic $^{87}\text{Sr}/^{86}\text{Sr}_{40\text{Ma}}$ and slighter less radiogenic $^{143}\text{Nd}/^{144}\text{Nd}_{40\text{Ma}}$. One group trends from the most radiogenic basalt (MS3) towards less radiogenic $^{143}\text{Nd}/^{144}\text{Nd}_{40\text{Ma}}$ and shows an evolving trend until rhyolite (MS11). The sills are part of this trend. Another group of lavas of variable compositions from trachybasalt to rhyolite plot separately at lower $^{143}\text{Nd}/^{144}\text{Nd}_{40\text{Ma}}$ (< 0.51255). The dyke plots in between the two groups, while the adakitic intrusives show little variation in Nd isotopes with respect to differentiation.

In the Pb isotopic space, the lavas and dyke plot in a cluster between $^{206}\text{Pb}/^{204}\text{Pb}_{40\text{Ma}}$ 18.42–18.64; $^{207}\text{Pb}/^{204}\text{Pb}_{40\text{Ma}}$ 15.6–15.64, and $^{208}\text{Pb}/^{204}\text{Pb}_{40\text{Ma}}$ 38.44–38.70 (Fig. 6B, C). Sills are shifted towards more radiogenic compositions ($^{206}\text{Pb}/^{204}\text{Pb}_{40\text{Ma}}$ 18.90–19.17; $^{207}\text{Pb}/^{204}\text{Pb}_{40\text{Ma}}$ 15.64–15.68, and $^{208}\text{Pb}/^{204}\text{Pb}_{40\text{Ma}}$ 38.97–39.33). Adakitic intrusives form a third cluster bracketed by the sills' compositions in $^{206}\text{Pb}/^{204}\text{Pb}_{15.7\text{Ma}}$ and $^{208}\text{Pb}/^{204}\text{Pb}_{15.7\text{Ma}}$, but are slightly more radiogenic in $^{207}\text{Pb}/^{204}\text{Pb}_{40\text{Ma}}$ (15.7–15.72; Fig. 6B, C). All rocks show compositions significantly more evolved than the NHRL (Zindler and Hart, 1986). In both the Pb-Pb plots, the samples depict a trend between depleted mantle compositions and the EMII mantle end-member, almost overlapping with the latter.

3.2. Radiometric dating

CL and BSE images are provided in supplementary file S12. Most zircons (>95%) are euhedral and prismatic, with aspect ratios ranging from 2 to 3, but some stubby and near-equidimensional grains are also present. Very few grains are broken, and internal fractures are rare. They are divided into 2 size groups on different mounts: smaller grains ~50 μm wide, and bigger grains ~100 μm wide. The zircons generally show clear oscillatory growth zoning in CL. Only a few grains show textures indicative of recrystallization obliterating earlier growth zoning. One grain shows a potential inherited core (MT25–29). Inclusions of other phases are rare (e.g., MT25-big-35). One grain (MT25-big-65) is not prismatic, but instead shows growth in 4 directions.

We analysed 229 zircon spots for sample MT25. Only 1 spot was rejected for MT25. Isotopes measured were ^{204}Pb , ^{206}Pb , ^{207}Pb and ^{238}U . In view of the expected very young age, ^{238}U was not measured, but calculated using a constant $^{238}\text{U}/^{235}\text{U}$ ratio of 137.88. Discordancy was calculated as the relative deviation between the $^{207}\text{Pb}/^{235}\text{U}$ and

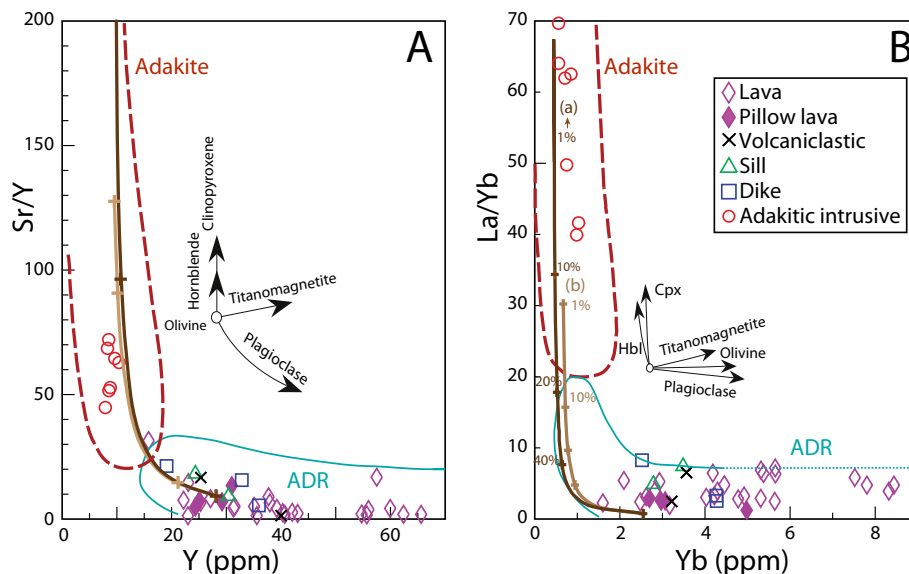


Fig. 5. Adakite versus normal arc volcanic rocks discrimination diagrams (Castillo, 2012). (A). Sr/Y vs. Y, (B). La/Yb vs. Yb.

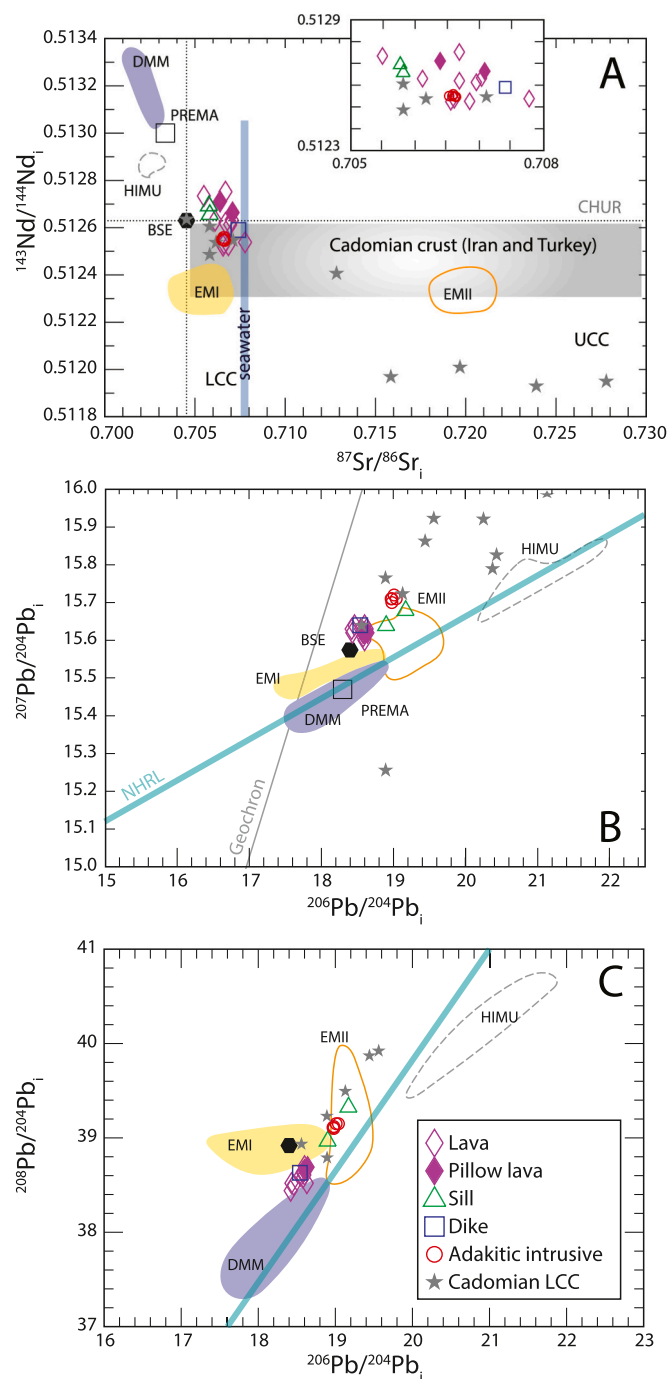


Fig. 6. Sr-Nd-Pb isotopic compositions. (A). $^{143}\text{Nd}/^{144}\text{Nd}_i$ versus $^{87}\text{Sr}/^{86}\text{Sr}_i$. (B). $^{207}\text{Pb}/^{204}\text{Pb}_i$ versus $^{206}\text{Pb}/^{204}\text{Pb}_i$. (C). $^{208}\text{Pb}/^{204}\text{Pb}_i$ versus $^{206}\text{Pb}/^{204}\text{Pb}_i$. DMM; depleted MORB mantle, PREMA; prevalent mantle, HIMU; high $^{238}\text{U}/^{204}\text{Pb}$ domain, BSE; bulk silicate earth, EM; enriched mantle, CHUR; chondritic uniform reservoir.

$^{206}\text{Pb}/^{238}\text{U}$ ages. 170 analyses showed <10% discordancy. ^{204}Pb was overall low, with $^{206}\text{Pb}/^{204}\text{Pb}$ ranging from 40 to >1000 at a mean of ~200. We discarded 5 points with >70% discordancy between the two U-Pb ages.

A histogram of the $^{206}\text{Pb}/^{238}\text{U}$ ages for sample MT25 shows a clear peak just below 16 Ma (Fig. 7). The distribution is asymmetric, but further analysis showed that ages >18 Ma are caused by relatively low $^{206}\text{Pb}/^{204}\text{Pb}$ values in the range 40–110. The remaining points give an age of 15.7 ± 0.1 Ma ($n = 183$, 2σ standard error of the mean; Fig. 7D), i. e., Miocene. Only 2 analyses from the grain with a deviating core

(MT25–29) are significantly older, namely ~29 and ~39 Ma, but the lower age spot has relatively high common lead, similar to other points rejected, and may represent an outlier from the main population.

4. Discussion

4.1. Biostratigraphy

We re-evaluated the ages of the Eocene succession based on the list of larger benthic foraminifera presented by Hadjian et al. (1970). The overall assemblage from E1 to E6 indicates an Eocene (56–33.9 Ma) age, with most of the succession likely of middle to upper Eocene age (47.8–33.9 Ma). At a generic level the taxa are distinct and clearly determinable in petrological thin section, thus, these identifications are likely robust. Whilst the species level determinations given in Hadjian et al. (1970) may be correct, in some cases the co-occurrence of species whose ranges are not known to overlap in the Western Tethyan region casts some doubt (e.g., in E3 *Nummulites globulus*, *Nummulites aturicus* and *Heterostegina*), and without the original sections or images there is no way to know whether these are correct. However, given that many of the larger benthic foraminiferal limestones in the succession are present within tuff or between igneous rocks, there is potential for independent dating of ranges of larger benthic foraminiferal taxa and improving overall biostratigraphy.

4.2. Geodynamic setting of Eocene volcanic rocks in the Tafresh area

Compared to the Miocene intrusives around Tafresh, the Eocene volcanic rocks have been relatively less well-studied. Available ages for the volcanic succession are conflicting, as summarised in Table 1. Verdel et al. (2011) find the oldest ages for zircons from an andesite flow near the bottom of the volcanic succession, in unit E2, around the Paleocene-Eocene boundary (54.7 ± 3.1 Ma). A green tuff bed slightly further up provides statistically indistinguishable ages based on Ar-Ar dating (56.6 ± 3.9 Ma). These ages are in relatively good agreement with the biostratigraphic constraints of Hadjian et al. (1970), and indicate that volcanism started around the early Eocene. In contrast, Ghorbani et al. (2014) found K/Ar ages of lavas in unit E2 of late Oligocene age; 26.8 ± 10.8 Ma and 26.0 ± 1.6 Ma. These authors consequently interpreted the volcanic succession to be of Oligocene to Miocene age, instead of Eocene. We note that one of these ages has a very large error, which could explain some of the discrepancy. While the other age has a relatively small error, the age is around 30 million years younger than the Ar/Ar and U-Pb ages of Verdel et al. (2011) and also conflicts with the biostratigraphy (Hadjian et al., 1970). We hypothesise that this discrepancy could be related to argon loss, and we do not consider the late Oligocene ages to accurately reflect the age of volcanism near Tafresh.

Our study of Eocene volcanic rocks shows that they have a geochemistry that is consistent with a subduction-related origin (Fig. 3B, C), in accordance with the findings of Ghorbani and Bezenjani (2011) these are non-adakitic rocks. The abundance of dacitic and rhyolitic products and the generally high-K character of the lavas (S8) are common observations in mature continental arc settings (Richards et al., 2012). Plagioclase fractionation seems to have played a prominent role in the evolution of the Eocene volcanic succession, as testified by the negative Eu anomaly in the more evolved lavas, and by trace element systematics (fractionation trends shown qualitatively in Fig. 4 and S13). Experimental glass compositions produced during fractional crystallization experiments by Nandedkar et al. (2014) from hydrous (3 wt% H₂O) arc basalt at 0.7 GPa and at $f\text{O}_2$ slightly above the NNO buffer (+0.3 to +1.07) are reported in Fig. 3C–G. Nandedkar et al. obtained a mineral assemblage compatible with that observed in our rocks, but their experiments depict a clear-cut calc-alkaline trend, which is followed by only some of our analysed Eocene lavas. Sisson et al. (2005) showed that partial melting of variably potassic arc basalts in the same

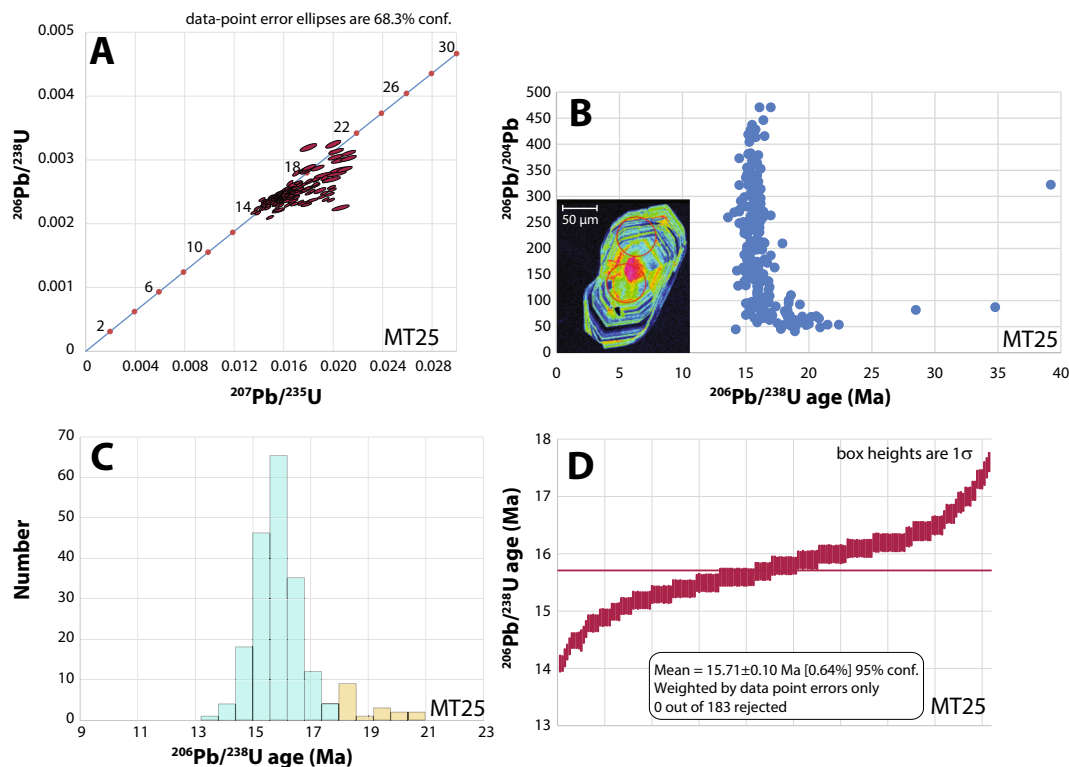


Fig. 7. (A). U-Pb concordia diagram showing a large concordant cluster of 1σ error ellipses located between 14 and 18 Ma, with 20–30 points scattered at higher values. (B). $^{206}\text{Pb}/^{204}\text{Pb}$ ratio versus $^{206}\text{Pb}/^{238}\text{U}$ ages (Ma), showing that ages >18 Ma are related to low $^{206}\text{Pb}/^{204}\text{Pb}$, i.e. have high inherited lead; the single value close to 40 Ma is valid. (C). Histogram showing all 221 data points below 21 Ma, with a peak close to 16 Ma. (D). $^{206}\text{Pb}/^{238}\text{U}$ values from 183 data points within their 1σ analytical uncertainties, sorted in increasing order. All methods shown indicate an age range 15.7–15.8 Ma. The high MSWD value of 21 is due to the program Glitter assigning unrealistically low uncertainties per data point. The final value is 15.71 ± 0.10 Ma (2σ standard error of the mean).

conditions as Nandedkar et al. (2014) can produce rhyolites of compositions akin to those of our most evolved samples. What stems from these comparisons is that the Eocene suite cannot be fully described by closed-system fractional crystallization processes from a single starting composition. Multiple parental melts are required for the least and most evolved lavas, and open-system processes such as magma mixing or crustal assimilation likely occurred, as suggested by plagioclase zoning and by the Sr-Nd isotopes. This is not surprising in a context of magmatic flare-up such as that of the Eocene of Iran, and for a volcano-sedimentary sequence produced over at least 12 million years. Crustal contamination likely played a role in the evolution of this volcanic suite as reflected by the position of these rocks between mantle values and the Cadomian crust realm in Sr-Nd isotope space (Fig. 6A) and the correlation between $^{143}\text{Nd}/^{144}\text{Nd}_{40\text{Ma}}$ and differentiation indexes (although not supported by $^{87}\text{Sr}/^{86}\text{Sr}_{40\text{Ma}}$ and $^{206}\text{Pb}/^{204}\text{Pb}_{40\text{Ma}}$, S14). Seawater or hydrous crustal fluids are capable of modifying Sr isotopes but not Nd isotopes. We suggest that the relatively large spread in Sr isotopes is best explained by interaction with crustal fluids with high highly radiogenic Sr. The Eocene volcanic succession was emplaced in a shallow marine basin, making interaction with seawater likely. However, seawater is not radiogenic, nor Sr-rich enough (Sr concentration of only 7.9 ppm, and $^{87}\text{Sr}/^{86}\text{Sr}$ ca. 0.708 in the Eocene; Charisi and Schmitz, 1995) to modify the Sr signatures of the volcanics up to the observed values. Fluid-mediated contamination is also supported by the fact that there is no correlation between $^{87}\text{Sr}/^{86}\text{Sr}_{40\text{Ma}}$ and differentiation indexes (such as MgO, SiO_2 , Zr), whereas the lava samples split into two groups when $^{143}\text{Nd}/^{144}\text{Nd}_{40\text{Ma}}$ is plotted against Nd concentrations (or other differentiation indexes). A more detailed study of the petrogenesis of the Eocene volcanics is not the main focus of this contribution, so we limit the discussion here to report that petrographically and geochemically the newly sampled rocks represent a typical comagmatic suite in a mature continental arc setting, and their geochemical signatures are

markedly different from those observed in the younger phase of intrusive rocks. For a more detailed discussion on petrography and alteration in the Tafresh area, we refer to Salari et al. (2021).

4.3. Adakitic intrusives from Tafresh area: lower crustal signature

To test the presence of adakitic signatures in our samples, we used the list of criteria of 10 different studies as summarised in Castillo (Castillo, 2012; see Table 2). None of the Eocene volcanic rocks, sills or dykes show adakitic signatures. Conversely, all of the porphyritic bodies show adakitic signatures, but there is some variation depending on which criteria are used (Table 2). The criteria of Castillo (2012) and Defant and Drummond (1993) flag all the 7 intrusive rocks sampled as adakitic. The rocks can be classified as high-silica adakitic rocks, following the criteria of Martin et al., 2005; (Fig. 8). High-silica adakites are petrogenetically different from low-silica ones, in that they do not necessarily represent melts of young subducted oceanic crust, although they might represent differentiated products of “true”, low-silica adakites (Castillo, 2012). There is general consensus that they might instead represent lower crustal melts, either produced by overthickened crust, or by foundering lower crust as also demonstrated experimentally (Qian and Hermann, 2013). Our adakitic intrusive rocks overlap well with experimental melts of mafic lower crust between 1 and 1.5 GPa (Fig. 8; Qian and Hermann, 2013). Other trace element signatures also argue in favour of a lower crustal origin for the Tafresh adakitic rocks, such as relatively high Rb/Sr (ca. 0.1 vs. 0.01 in MORBs) and La/Sm (ca. 8.5–12.7 vs. 0.95 in MORBs), and relatively low Nb/U (<5 vs. 38–40 in MORBs) with respect to MORB (Sun and McDonough, 1989), taken as representative of the subducting oceanic crust. Ultimately, however, a slab-derived origin can be discarded based on the isotopic signatures, as discussed further below.

Our adakitic rocks from Tafresh plot within the range of Sr, Nd and

Table 2
Criteria of the different adakite tests (Castillo, 2012; Danyushevsky et al., 2008; Defant and Drummond, 1990; Defant and Kepezhnikas, 2001; Hastie et al., 2010; Martin, 1999; Richards and Kerrich, 2007; Sajona et al., 1993; Yagodinski and Kelemen, 1998) and number of adakites in the literature compilation and our Tafresh dataset.

	SiO ₂	Al ₂ O ₃	MgO	Na ₂ O	Sr	Y	Yb	Ni	Cr	Sr/Y	La/Yb	# Adakites in compilation	Notes	# Adakites in our dataset
Defant and Drummond, 1990	≥56	≥15	<3, >6		≥400	<18	≤1.9			≥20	≥8	521		6
Defant and Drummond, 1993		≥15			≥350	≤18	≤1.9			≥32	≥8	759		7
Sajona et al., 1993		>14.5	<3	3.0-7.4	>1170	≤14	≤1.4	9-45	14-66			108	(29 miss one characteristic, mostly MgO)	0
Yagodinski and Kelemen, 1998			>4.4				<1	20-40	30-50		>17	0		0
Martin, 1999	>56			3.5-7.5	300-2000	≤18	≤1.8					25		0
Defant and Kepezhnikas, 2001	>56	>15	<3	>3.5	>400	≤18	≤1.9	≥20	≥30	≥40	≥20	402		4
Richards and Kerrich, 2007				≥3.5	≥400	≤18	≤1.9	≥20	≥30	≥20	≥20	94		0
Danyushevsky et al., 2008	>65	>15	1-5	4-5	780-1700	10-36	<1.7	10-114	8-140	>120	>30	1	(24 miss one characteristic, mostly Sr/Y)	0
Hastie et al., 2010	≥56	≥15	≤2	>3.8	>66	<13	<0.9	≤30	≤40	>7	>5	96		0
Castillo, 2012			<3	>3	>300	<10	<1			>20	>20	250		5

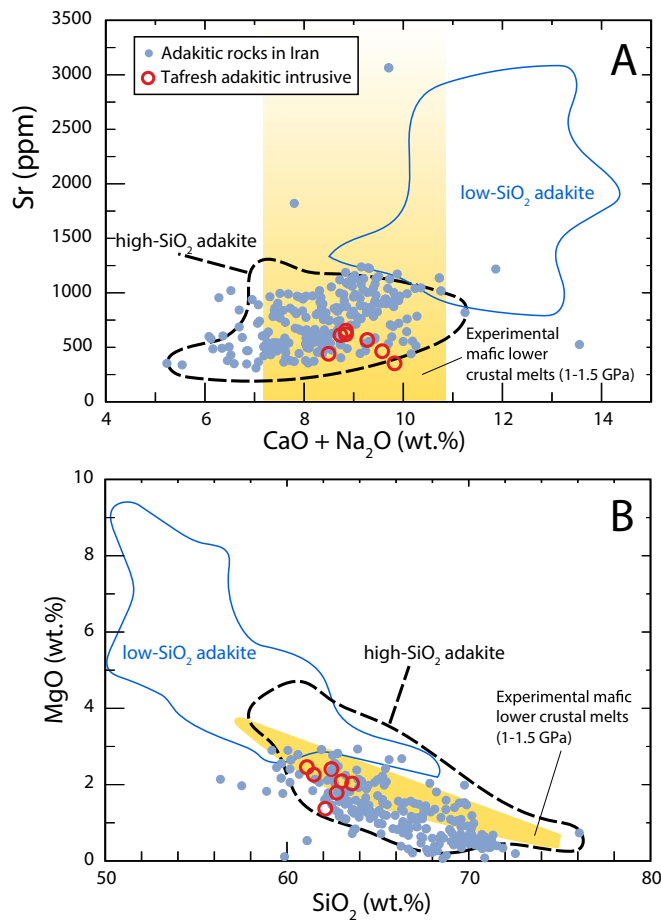


Fig. 8. High versus low silica adakitic rocks based on (A). Sr versus CaO + Na₂O and (B). MgO versus SiO₂ with experimental mafic lower crustal melts (Qian and Hermann, 2013).

Pb isotopic values reported for mafic Cadomian crust (Sepidbar et al., 2020; Fig. 6), which is thought to represent the basement in the area. Recycling of Cadomian crust (with an age of ~550 Ma; Moghadam et al., 2015) is often inferred in Iran. Chaharlang and Ghorbani (2020) show that in addition to Carboniferous and Cadomian zircons, the Tafresh volcanic rocks contain Paleoproterozoic (~2380 Ma) zircons. We stress that -since the adakitic melts are significantly enriched in Sr (353–652 ppm), Nd (22–30 ppm) and Pb (20–51 ppm)- they are less prone to contamination during their ascent and emplacement in the crust, hence their isotopic traits likely reflect those of the source. The very uniform Sr, Nd and Pb isotope ratios in the adakitic rocks suggest a homogenous source that might not have been subsequently disturbed by open-system processes. The highly fractionated LREE/HREE (e.g. La/Yb 40–70; Fig. 5) strongly support melting in presence of residual garnet. Comparing the compositions of our adakitic rocks with melting curves calculated by Castillo, 2012 (Fig. 5A, B), we find a best fit with 1–10% partial melting of eclogite (50:50 pyroxene:garnet), or up to 1% melting of garnet amphibolite (25:75 garnet:amphibole), followed by fractional crystallization of clinopyroxene and amphibole with a starting N-MORB trace element composition (Sun and McDonough, 1989). Although high Sr/Y and La/Yb ratios could be produced or enhanced by amphibole and clinopyroxene fractionation, the La/Yb ratios in these rocks are so high that the presence of residual garnet in the source is required. The lack of some trace element data (Cr, Ni) precludes more detailed investigations on the petrogenesis of these rocks. However, the displayed geochemical characteristics point strongly towards a predominantly lower crustal signal in the source of these melts (e.g. Castillo, 2012). Previous studies on adakitic rocks from Iran suggested a similar origin (e.g. Torkian et al.,

2019). Our geochemical data currently do not allow us to assess whether this is founded or thickened lower crust. Following the suggestion of Castillo (2012), these rocks should be referred to as adakitic, rather than proper adakites, as they lack evidence for slab melting.

4.4. Adakitic signatures in Iran: literature compilation and age progression

We compiled bulk rock geochemical data from >150 studies of Mesozoic and younger igneous rocks in Iran (S15), with data from over 3500 samples. We tested the presence of adakites using the 10 different criteria as summarised in the review of Castillo (2012). Depending on which criteria are used, between 0 and 759 samples are defined as adakitic (see Table 2). As Castillo (2012) provides an extensive review of the different criteria for adakites, we proceed with the set of 9 characteristics as laid out by Castillo (2012). Literature compilations are always incomplete, as new studies are published continuously. Furthermore, geochemical studies do not always provide complete element datasets, and some studies might not present data that are critical for performing these standardised adakite tests. We found that Cr and Ni data were missing for a significant number of samples, while Yb and La were reported for the majority of samples, but not all. This lack of data could potentially lead to an underestimation of the true number of adakitic rocks in our compilation. Our assessment of the number of adakitic rocks in Iran is thus likely a minimum estimate. However, we consider our compilation sufficiently large to provide a good overview of Mesozoic and younger adakitic rocks in Iran and the different areas where they occur. On the plot of Sr/Y versus Y, all adakitic rocks in our compilation plot within the adakite field (S16), most fall within the range of high-Si adakites (Fig. 8). Primitive-mantle normalised (Sun and McDonough, 1989) incompatible trace element diagrams grouped by region are shown in Supplementary File S17. The Alborz Mountains appear to stand out as a region that lacks adakitic signatures (see also Fig. 1B). We suggest that this is not due to sampling bias, as a relatively large number of samples in our compilation (>250) come from this area. The Sanandaj-Sirjan Zone (SSZ) is sampled mostly at its north-western end and shows adakitic signatures of predominantly Paleocene age (66–56 Ma). In the Lut Block, central Iran and northeast Iran, adakitic rocks are mostly of Paleogene (66–34 Ma) age.

In the Tafresh area, the literature offers conflicting information about adakitic signatures and ages, which need to be carefully evaluated. Ghorbani and Bezenjani (2011) report adakitic signatures for 6 of their samples: T1, T2, T3, T5, T6 and T11. Using the Castillo (2012) criteria, samples T1, T3, T5 and T11 are classified as adakitic. When using Defant and Drummond (1993) criteria, samples T8 and T9 samples are also classified as adakitic. Ghorbani and Bezenjani (2011) posited that their adakitic rocks were from the Eocene volcanic phase, but in their conclusions note that adakitic signatures are from dykes and stocks. While Ghorbani et al. (2014) interpret the volcanic succession to have an Oligocene to Miocene age, they indicated that their adakitic sample TF5 (presumably sample T5 from Ghorbani and Bezenjani, 2011), is from a dyke or sill. Our investigation finds no adakitic signatures in dykes, nor in the Eocene volcanic succession, but only in intrusive porphyritic bodies. We obtained a U-Pb age of 15.7 ± 0.1 Ma (Miocene) for the porphyritic body intruded into unit E4. We consider it most likely that the adakitic rock (T5/TF5) from Ghorbani and Bezenjani (2011) and Ghorbani et al. (2014) was obtained not from the volcanic succession, but rather represents the intrusive phase that postdates Eocene volcanism. The 15.7 Ma age that we obtained in our study is younger than the 19–20 Ma ages obtained by Mirnejad et al. (2019) for granitic intrusions nearby. Although Mirnejad et al. specifically mention that their samples from the granitoids do not exhibit adakitic signatures (based on Sr/Y vs Y ratios), some of their samples do in fact classify as adakitic, according to Defant and Drummond (1990) criteria (samples GH5 and GH9, other samples score 3–5 out of 6 characteristics), as well as according to the Defant and Drummond (1993) criteria (samples GH2,

GH3, GH6 and GH9, other samples score 1–4 out of 5 characteristics). Also Raeisi et al. (2020) have one adakitic sample according to Defant and Drummond (1990) (G5) and Defant and Drummond (1993; GH6).

Until now, an age progression in adakitic rock occurrences along the Neotethys arc was unclear due to the presence of an outlier (see Fig. 1B): the Tafresh adakitic rocks. Our study shows that the age of the Tafresh adakitic rocks should be reinterpreted. Our new 15.7 Ma U-Pb zircon age suggests that the adakitic rocks near Tafresh do not represent an Eocene outlier, but instead, with their Miocene age, fit well into a trend in which adakitic rocks become younger towards the southeast of Iran (see Fig. 9).

4.5. Adakites and the geodynamic evolution of the Neotethys arc

Even though the adakitic rocks near Tafresh show geochemical characteristics that indicate they have formed because of melting of the lower continental crust, and not a subducting slab, we hypothesise that progressive slab break-off could have provided a heating mechanism that led to melting of the lower continental crustal source (see Fig. 9). Eocene volcanic rocks in the former Neotethys arc show continental arc geochemical signatures (Verdel et al., 2011), and have generally been interpreted as produced by a continental arc that formed due to subduction of the Neotethys slab (Shafaii Moghadam et al., 2020). After the closure of the Neotethys and the collision between Arabia and Eurasia, arc volcanism ceased. This might have happened first in the northwest of Iran, where the oldest adakitic rocks have an age of early Oligocene (around 31 Ma, Fig. 9). As continental collision proceeded towards the southeast, arc volcanism ceased progressively in a southeastern direction. The age progression of adakitic rocks is in line with evidence for a diachronous Arabia-Eurasia collision from tectonic studies (e.g. Darin and Umhoefer, 2022). After collision, hot asthenosphere started to well up, possibly in relation to break-off of the Neotethys slab, which in turn provided sufficient heat for the lower continental crust and the enriched mantle wedge to melt, causing volcanism with adakitic signatures. We note that generation of adakitic magmas after this initial phase may have continued, and our scenario is focused on explaining the earliest phase of adakitic igneous activity along the Neotethys arc. Furthermore, adakitic rocks outside of the Neotethys arc likely had other mechanisms of generation, and further assessment is beyond the scope of this study.

Our literature compilation demonstrates a clear gap in the (western) Alborz Mountains, where no adakitic rocks have yet been found. Van der Boon (2017) hypothesised that this area was underlain by a flatter slab, which explains a larger distance between the Alborz Eocene volcanics and the Neotethys trench. Our present study shows that there is no geochemical evidence in the form of adakitic rocks for the slab-tear that was also inferred in the van der Boon (2017) scenario. With our current data, we cannot constrain whether the absence of adakitic rocks in the Alborz Mountains is a consequence of sampling bias, or has a geodynamic explanation, but future studies may solve this problem.

5. Conclusions

The Tafresh adakitic rocks were previously interpreted as Eocene in age and thus formed an outlier from the trend of adakitic rocks that are younging towards the southeast of Iran. We show, on the basis of geochemical data of Eocene volcanic rocks and Miocene intrusive rocks that the adakitic signature is only present in the Miocene intrusive rocks. These adakitic intrusive rocks have an age of 15.7 Ma, based on our new U-Pb zircon ages. Eocene rocks show continental arc signatures and are not adakitic. The Miocene adakitic rocks occur in porphyritic bodies that were most likely generated by melting of lower continental crust, and not by slab melting. Adakitic rocks are present across Iran, and show consistent age distributions. In the Neotethys arc, they postdate voluminous Eocene arc magmatism, and are thus related to a separate process. We hypothesise that after Arabia-Eurasia continental collision, the Neotethys slab broke off, and upwelling of hot asthenosphere caused melting of the lower continental crust, which led to the generation of

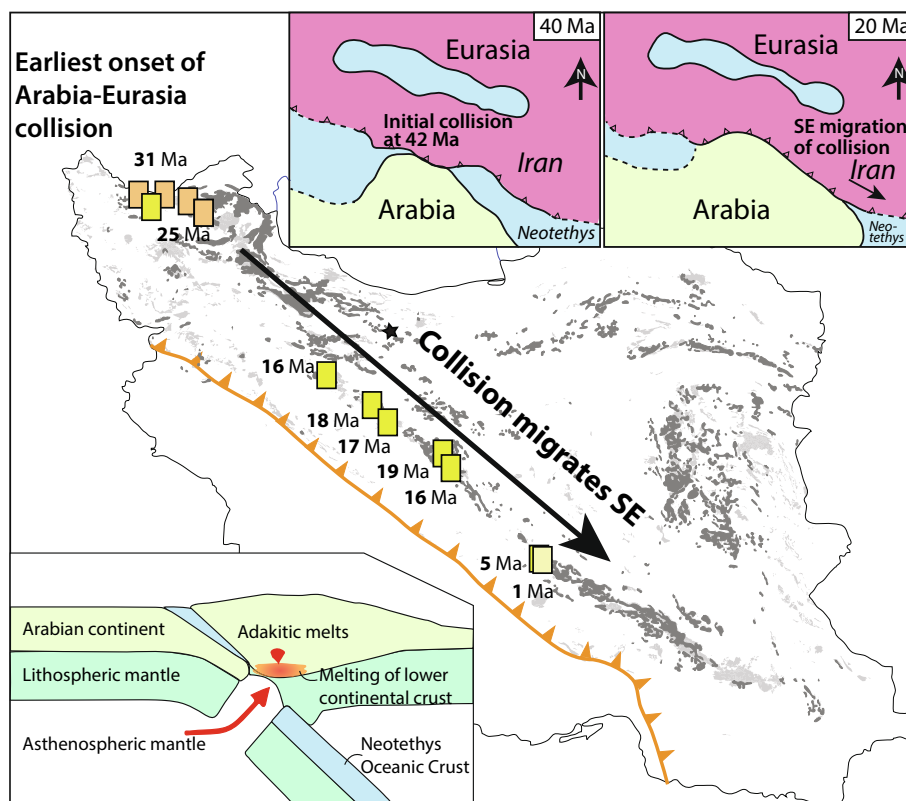


Fig. 9. Summary of ages of adakitic rocks in Iran along the former Neotethys arc. Top right cartoons show the tectonic reconstruction of the Arabia–Eurasia collision zone at 40 and 20 Ma (modified after [Darin and Umhoefer, 2022](#)). Bottom left shows the hypothesised scenario for adakitic melt generation by heating of the lower continental crust by upwelling hot asthenosphere after slab break-off (modified after [Honarmand et al., 2014](#)).

adakitic magmas. Adakitic rocks along the former Neotethys arc show a progression in age, becoming younger towards the southeast of Iran. This fits well with a diachronous collision and slab break-off in the Arabia-Eurasia collision zone, starting in the northwest of Iran and progressing to the southeast.

CRediT authorship contribution statement

Annie van der Boon: Writing – review & editing, Writing – original draft, Visualization, Validation, Supervision, Investigation, Formal analysis, Data curation, Conceptualization. **Marjolein N. Naudé:** Writing – original draft, Visualization, Investigation, Formal analysis, Data curation, Conceptualization. **Sara Callegaro:** Writing – review & editing, Writing – original draft, Visualization, Validation, Investigation, Formal analysis, Data curation. **Iman Monsef:** Writing – original draft, Supervision, Investigation, Data curation, Conceptualization. **Mahnaz Rezaeian:** Writing – original draft, Supervision, Project administration, Investigation, Data curation, Conceptualization. **Ali Niknam:** Writing – original draft, Supervision, Investigation, Data curation, Conceptualization. **Laura J. Cotton:** Writing – original draft, Investigation, Formal analysis, Conceptualization. **Petrus le Roux:** Writing – original draft, Supervision, Methodology, Investigation, Formal analysis, Data curation. **Leo M. Kriegsman:** Writing – review & editing, Writing – original draft, Validation, Supervision, Methodology, Formal analysis, Data curation. **Paul R.D. Mason:** Writing – review & editing, Writing – original draft, Supervision, Investigation, Formal analysis, Data curation, Conceptualization. **Cor G. Langereis:** Writing – original draft, Supervision, Project administration, Investigation, Funding acquisition, Data curation, Conceptualization.

Declaration of competing interest

The authors declare that they have no known competing financial interests or personal relationships that could have appeared to influence the work reported in this paper.

Acknowledgements

We thank Daniël Bakker for help in compiling the literature database. AvdB and SC acknowledge financial support from The Research Council of Norway through its Centres of Excellence Scheme, project number 332523 (PHAB). AvdB also acknowledges Research Council of Norway project number 334622 (Young Talent Scheme, project PANDA). SC also acknowledges Research Council of Norway project number 301096 (Young Talent Scheme, project MAPLES). We thank editor Di-Cheng Zhu, Hadi Shafaii Moghadam, Kwan-Nang Pang and one anonymous reviewer for insightful comments that have improved this manuscript.

Appendix A. Supplementary data

Supplementary data to this article can be found online at <https://doi.org/10.1016/j.lithos.2024.107737>.

References

- Abdi, M., Karimpour, M.H., 2013. Petrochemical characteristics and timing of middle Eocene granitic magmatism in Kooh-Shah, Lut Block, Eastern Iran. *Acta Geol. Sin. Engl. Ed.* 87, 1032–1044. <https://doi.org/10.1111/1755-6724.12108>.
- Agard, P., Omrani, J., Jolivet, L., Whitechurch, H., Vrielynck, B., Spakman, W., Monié, P., Meyer, B., Wortel, R., 2011. Zagros orogeny: a subduction-dominated process. *Geol. Mag.* 148, 692–725. <https://doi.org/10.1017/S001675681100046X>.
- Aghazadeh, M., Castro, A., Badrzadeh, Z., Vogt, K., 2011. Post-collisional polycyclic plutonism from the Zagros hinterland: the Shaivar Dagh plutonic complex, Alborz

- belt, Iran. *Geol. Mag.* 148, 980–1008. <https://doi.org/10.1017/S0016756811000380>.
- Agmini, C., Fornaciari, E., Giusberti, L., Grandesso, P., Lanci, L., Luciani, V., Muttoni, G., Pälke, H., Rio, D., Spofforth, D.J.A., Stefani, C., Palike, H., Rio, D., Spofforth, D.J.A., Stefani, C., 2011. Integrated biomagnetostratigraphy of the Alano section (NE Italy): a proposal for defining the middle-late Eocene boundary. *Geol. Soc. Am. Bull.* 123, 841–872. <https://doi.org/10.1130/B30158.1>.
- Alai Mahabadi, S., Kohansal, R., Ghomian, Y., Soltani, M.V., 2000. *Salafchegan-Khorhe* Geol. Map. Iran. Geological Survey of Iran, 1:100 000 Ser., Sheet 6058.
- Alirezai, S., Einali, M., Jones, P., Hassanpour, S., Arjmandzadeh, R., 2016. Mineralogy, geochemistry, and evolution of the Mivehrood skarn and the associated pluton, Northwest Iran. *Int. J. Earth Sci.* 105, 849–868. <https://doi.org/10.1007/s00531-015-1200-4>.
- Ao, S., Xiao, W., Khalatbari Jafari, M., Talebian, M., Chen, L., Wan, B., Ji, W., Zhang, Z., 2016. U–Pb zircon ages, field geology and geochemistry of the Kermanshah ophiolite (Iran): From continental rifting at 79 Ma to oceanic core complex at ca 36 Ma in the southern Neo-Tethys. *Gondwana Res.* 31, 305–318. <https://doi.org/10.1016/j.gr.2015.01.014>.
- Asiabanha, A., Foden, J., 2012. Post-collisional transition from an extensional volcano-sedimentary basin to a continental arc in the Alborz Ranges, N-Iran. *Lithos* 148, 98–111. <https://doi.org/10.1016/j.lithos.2012.05.014>.
- Ayati, F., 2015. Geochemistry investigations of volcanic rocks in Salafchegan – Khorhe sheet with emphasize on Sr-Nd isotopic data. *J. Tethys* 3, 163–181.
- Azizi, H., Najari, M., Asahara, Y., Catlos, E.J., Shimizu, M., Yamamoto, K., 2015. U-Pb zircon ages and geochemistry of Kangarah and Taghiabad mafic bodies in northern Sanandaj-Sirjan Zone, Iran: evidence for intra-oceanic arc and back-arc tectonic regime in Late Jurassic. *Tectonophysics* 660, 47–64. <https://doi.org/10.1016/j.tecto.2015.08.008>.
- Azizi, H., Stern, R.J., Topuz, G., Asahara, Y., Moghadam, H.S., 2019. Late Paleocene adakitic granitoid from NW Iran and comparison with adakites in the NE Turkey: Adakitic melt generation in normal continental crust. *Lithos* 346–347, 105151. <https://doi.org/10.1016/j.lithos.2019.105151>.
- Babazadeh, S., Raeisi, D., D'Antonio, M., Zhao, M., Long, L.E., Cottle, J.M., Modabber, S., 2022. Petrogenesis of Miocene igneous rocks in the Tafresh area (central Urumieh-Dokhtar magmatic arc, Iran): Insights into mantle sources and geodynamic processes. *Geol. J.* 57, 2884–2903. <https://doi.org/10.1002/gj.4451>.
- Badr, M.J., Collins, A.S., Masoudi, F., Cox, G., Mohajjel, M., 2013. The U-Pb age, geochemistry and tectonic significance of granitoids in the Soursat complex, Northwest Iran. *Turk. J. Earth Sci.* 22, 1–31. <https://doi.org/10.3906/yer-1001-37>.
- Castillo, P.R., 2012. Adakite petrogenesis. *Lithos* 134–135, 304–316. <https://doi.org/10.1016/j.lithos.2011.09.013>.
- Castro, A., Aghazadeh, M., Badrzadeh, Z., Chichorro, M., 2013. Late Eocene-Oligocene post-collisional monzonitic intrusions from the Alborz magmatic belt, NW Iran. An example of monzonite magma generation from a metasomatized mantle source. *Lithos* 180–181, 109–127. <https://doi.org/10.1016/j.lithos.2013.08.003>.
- Chaharlang, R., Ghorbani, M.R., 2020. A hidden crust beneath the central Urumieh-Dokhtar Magmatic Arc revealed by inherited zircon ages, Tafresh, Iran. *Geol. J.* 55, 3770–3781. <https://doi.org/10.1002/gj.3631>.
- Charis, S.D., Schmitz, B., 1995. Stable ($\delta^{13}\text{C}$, $\delta^{18}\text{O}$) and strontium ($^{87}\text{Sr}/^{86}\text{Sr}$) isotopes through the Paleocene at Gebel Aweina, eastern Tethyan region. *Palaeogeogr. Palaeoclimatol. Palaeoecol.* 116, 103–129. [https://doi.org/10.1016/0031-0182\(94\)00090-U](https://doi.org/10.1016/0031-0182(94)00090-U).
- Chiu, H.-Y., Chung, S.-L., Zarrinkoub, M.H., Mohammadi, S.S., Khatib, M.M., Iizuka, Y., 2013. Zircon U–Pb age constraints from Iran on the magmatic evolution related to Neotethyan subduction and Zagros orogeny. *Lithos* 162–163, 70–87. <https://doi.org/10.1016/j.lithos.2013.01.006>.
- Danyushevsky, L.V., Falloon, T.J., Crawford, A.J., Tetroeva, S.A., Leslie, R.L., Verbeeten, A., 2008. High-Mg adakites from Kadavu Island Group, Fiji, Southwest Pacific: evidence for the mantle origin of adakite parental melts. *Geology* 36, 499–502. <https://doi.org/10.1130/G24349A.1>.
- Darin, M.H., Umhoefer, P.J., 2022. Diachronous initiation of Arabia–Eurasia collision from eastern Anatolia to the southeastern Zagros Mountains since middle Eocene time. *Int. Geol. Rev.* 64, 2653–2681. <https://doi.org/10.1080/00206814.2022.2048272>.
- Defant, M.J., Drummond, M.S., 1990. Derivation of some modern arc magmas by melting of young subducted lithosphere. *Nature* 347, 662–665. <https://doi.org/10.1038/347662a0>.
- Defant, M.J., Drummond, M.S., 1993. Mount St. Helens: potential example of the partial melting of the subducted lithosphere in a volcanic arc. *Geology* 21, 547–550. [https://doi.org/10.1130/0091-7613\(1993\)021<0547:MSHPEO>2.3.CO;2](https://doi.org/10.1130/0091-7613(1993)021<0547:MSHPEO>2.3.CO;2).
- Defant, M.J., Kepezhinskas, P., 2001. Evidence suggests slab melting in arc magmas. *EOS Trans. Am. Geophys. Union* 82, 65–69. <https://doi.org/10.1029/01E000038>.
- Emami, M.H., 1981. *Géologie de la Région de Quom-Aran (Iran). Contribution à l'étude Dynamique et Géochimique du Volcanisme Tertiaire de l'Iran Central (Thesis). Université Joseph-Fourier - Grenoble I (in French)*, tel-00509888v2.
- Flandrin, J., Hadjian, J., 1970. L'Éocène de la région de Tafresh (Nord-Ouest de l'Iran central). *Bull. Société Géologique Fr. (7)XII*, 826–833. <https://doi.org/10.2113/gssgfbull.s7-xii.5.826>.
- Ghadami, G., Shahre Babaki, A.M., Mortazavi, M., 2008. Post-collisional Plio-Pleistocene adakitic volcanism in Central Iranian volcanic belt: geochemical and geodynamic implications. *J. Sci. Islam. Repub. Iran* 19, 223–235.
- Ghahamghash, J., Schmitt, A.K., Chaharlang, R., 2019. Age and compositional evolution of Sahand volcano in the context of post-collisional magmatism in northwestern Iran: evidence for time-transgressive magmatism away from the collisional suture. *Lithos* 344–345, 265–279. <https://doi.org/10.1016/j.lithos.2019.06.031>.
- Ghasemi, A., Tabatabaei Manesh, S.M., 2015. Geochemistry and petrogenesis of Gohroud Igneous complex (Urumieh-Dokhtar zone): evidence for Neotethyan subduction during the Neogene. *Arab. J. Geosci.* <https://doi.org/10.1007/s12517-015-1883-7>.
- Ghorbani, M.R., Bezenjani, R.N., 2011. Slab partial melts from the metasomatizing agent to adakite, Tafresh Eocene volcanic rocks, Iran. *Island Arc* 20, 188–202. <https://doi.org/10.1111/j.1440-1738.2010.00757.x>.
- Ghorbani, M.R., Graham, I.T., Ghaderi, M., 2014. Oligocene–Miocene geodynamic evolution of the central part of Urumieh-Dokhtar Arc of Iran. *Int. Geol. Rev.* 56, 1039–1050. <https://doi.org/10.1080/00206814.2014.919615>.
- Hadjian, J., Amini, B., Amini Chehragh, M.R., 1970. *Geological Map of Iran 1:100,000 Series Sheet 6059 - Tafresh*.
- Hastie, A.R., Kerr, A.C., McDonald, I., Mitchell, S.F., Pearce, J.A., Millar, I.L., Barford, D., Mark, D.F., 2010. Geochronology, geochemistry and petrogenesis of rhyodacite lavas in eastern Jamaica: a new adakite subgroup analogous to early Archaean continental crust? *Chem. Geol.* 276, 344–359. <https://doi.org/10.1016/j.chemgeo.2010.07.002>.
- Honarmand, M., Omran, N.R., Corfu, F., Emami, M.H., Nabatian, G., 2013. Geochronology and magmatic history of a calc-alkaline plutonic complex in the Urumieh – Dokhtar Magmatic Belt, Central Iran: Zircon ages as evidence for two major plutonic episodes. *N. Jb. Minerol. Abh. (J. Min. Geochem.)* 190, 67–77. <https://doi.org/10.1127/0077-7757/2013/0230>.
- Honarmand, M., Rashidnejad Omran, N., Neubauer, F., Hashem Emami, M., Nabatian, G., Liu, X., Dong, Y., von Quadt, A., Chen, B., 2014. Laser-ICP-MS U–Pb zircon ages and geochemical and Sr–Nd–Pb isotopic compositions of the Niyasar plutonic complex, Iran: constraints on petrogenesis and tectonic evolution. *Int. Geol. Rev.* 56, 104–132. <https://doi.org/10.1080/00206814.2013.820375>.
- Irvine, T.N., Baragar, W.R.A., 1971. A guide to the chemical classification of the common volcanic rocks. *Can. J. Earth Sci.* 8, 523–548.
- Jahangiri, A., 2007. Post-collisional Miocene adakitic volcanism in NW Iran: geochemical and geodynamic implications. *J. Asian Earth Sci.* 30, 433–447. <https://doi.org/10.1016/j.jseae.2006.11.008>.
- Kay, R.W., Mahlburg Kay, S., 1993. Delamination and delamination magmatism. *Tectonophysics* 219, 177–189. [https://doi.org/10.1016/0040-1951\(93\)90295-U](https://doi.org/10.1016/0040-1951(93)90295-U).
- Kheirkhah, M., Neill, I., Allen, M.B., Emami, M.H., Shahraki Ghadimi, A., 2020. Distinct sources for high-K and adakitic magmatism in SE Iran. *J. Asian Earth Sci.* 196, 104355. <https://doi.org/10.1016/j.jseae.2020.104355>.
- Le Maitre, R.W., Streckeisen, A., Zanettin, B., Le Bas, M.J., Bonin, B., Bateman, P. (Eds.), 2002. *Igneous Rocks: A Classification and Glossary of Terms, 2nd ed.* Cambridge University Press, Cambridge. <https://doi.org/10.1017/CBO9780511535581>.
- Martin, H., 1999. Adakitic magmas: modern analogues of Archaean granitoids. *Lithos* 46, 411–429. [https://doi.org/10.1016/S0024-4937\(98\)00076-0](https://doi.org/10.1016/S0024-4937(98)00076-0).
- Martin, H., Smithies, R.H., Rapp, R., Moyen, J.F., Champion, D., 2005. An overview of adakite, tonalite-trondhjemite-granodiorite (TTG), and sanukitoid: relationships and some implications for crustal evolution. *Lithos* 79, 1–24. <https://doi.org/10.1016/j.lithos.2004.04.048>.
- McDonough, W.F., Sun, S.-S., 1995. The composition of the Earth. *Chem. Geol. Chem. Evol. Mantle* 120, 223–253. [https://doi.org/10.1016/0009-2541\(94\)00140-4](https://doi.org/10.1016/0009-2541(94)00140-4).
- McQuarrie, N., van Hinsbergen, D.J.J., 2013. Retrodeforming the Arabia-Eurasia collision zone: age of collision versus magnitude of continental subduction. *Geology* 41, 315–318. <https://doi.org/10.1130/G33591.1>.
- Mirnejad, H., Lalonde, A.E., Obeid, M., Hassanzadeh, J., 2013. Geochemistry and petrogenesis of Mashhad granitoids: an insight into the geodynamic history of the Paleo-Tethys in northeast of Iran. *Lithos* 170–171, 105–116. <https://doi.org/10.1016/j.lithos.2013.03.003>.
- Mirnejad, H., Raeisi, D., McFarlane, C., Sheibi, M., 2019. Tafresh intrusive rocks within the Urumieh-Dokhtar Magmatic Arc: appraisal of Neo-Tethys subduction. *Geol. J.* 54, 1745–1755. <https://doi.org/10.1002/gj.3266>.
- Moghadam, H.S., Ghorbani, G., Zaki Khedr, M., Fazlnia, N., Chiaradia, M., Eyuboglu, Y., Santosh, M., Galindo Francisco, C., Lopez Martinez, M., Gourgand, A., Arai, S., 2014. Late Miocene K-rich volcanism in the Eslamieh Peninsula (Saray), NW Iran: implications for geodynamic evolution of the Turkish-Iranian High Plateau. *Gondwana Res.* 26, 1028–1050. <https://doi.org/10.1016/j.gr.2013.09.015>.
- Moghadam, H.S., Khademi, M., Hu, Z., Stern, R.J., Santos, J.F., Wu, Y., 2015. Cadomian (Ediacaran-Cambrian) arc magmatism in the ChahJam-Biarjmand metamorphic complex (Iran): magmatism along the northern active margin of Gondwana. *Gondwana Res.* 27, 439–452. <https://doi.org/10.1016/j.gr.2013.10.014>.
- Mokhtari, M.A.A., Moinvaziri, H., Ghorbani, M.R., Mehrpartou, M., 2010. Petrology and petrogenesis of Kamtal Intrusion Eastern Azarbaijan. *NW Iran. Cent. Eur. Geol.* 53, 79–96. <https://doi.org/10.1556/CEUGeol.53.2010.1.5>.
- Nandedkar, R.H., Ulmer, P., Müntener, O., 2014. Fractional crystallization of primitive, hydrous arc magmas: An experimental study at 0.7 GPa. *Contrib. Mineral. Petrol.* 167, 1015. <https://doi.org/10.1007/s00410-014-1015-5>.
- Nia, H.M., Baghban, S., Simmonds, V., 2017. Geology, geochemistry and petrogenesis of post-collisional adakitic intrusions and related dikes in the Khoynard area, NW Iran. *Chem. Erde* 77, 53–67. <https://doi.org/10.1016/j.chemer.2017.02.001>.
- Nouri, F., Azizi, H., Asahara, Y., Whattam, S.A., Tsuboi, M., Mohammad, Y.O., Minami, M., Anma, R., 2021. Coexistence of two types of late Paleocene adakitic granitoid, Soursat complex, NW Iran. *Lithos* 404–405, 106438. <https://doi.org/10.1016/j.lithos.2021.106438>.
- Omran, J., Agard, P., Whitechurch, H., Benoit, M., Prouteau, G., Jolivet, L., 2008. Arc-magmatism and subduction history beneath the Zagros Mountains, Iran: a new report of adakites and geodynamic consequences. *Lithos* 106, 380–398. <https://doi.org/10.1016/j.lithos.2008.09.008>.
- Pang, K.-N., Chung, S.-L., Hossein, M., Li, X.-H., Lee, H.-Y., Lin, T.-H., Chiu, H.-Y., 2016. New age and geochemical constraints on the origin of Quaternary adakite-like lavas

- in the Arabia-Eurasia collision zone. *Lithos* 264, 348–359. <https://doi.org/10.1016/j.lithos.2016.08.042>.
- Pearce, J.A., 1996. A user's guide to basalt discrimination diagrams. *Trace element geochemistry of volcanic rocks: applications for massive sulphide exploration*. Geological Association of Canada, *Short Course Notes* 12, 79–113.
- Peccerillo, A., Taylor, S.R., 1976. Geochemistry of eocene calc-alkaline volcanic rocks from the Kastamonu area, Northern Turkey. *Contrib. Mineral. Petrol.* 58, 63–81. <https://doi.org/10.1007/BF00384745>.
- Petrone, C.M., Ferrari, L., 2008. Quaternary adakite—Nb-enriched basalt association in the western Trans-Mexican Volcanic Belt: Is there any slab melt evidence? *Contrib. Mineral. Petrol.* 156, 73–86. <https://doi.org/10.1007/s00410-007-0274-9>.
- Qian, Q., Hermann, J., 2013. Partial melting of lower crust at 10–15 kbar: Constraints on adakite and TTG formation. *Contrib. Mineral. Petrol.* 165, 1195–1224. <https://doi.org/10.1007/s00410-013-0854-9>.
- Raeisi, D., Mirnejad, H., McFarlane, C., Sheibi, M., Babazadeh, S., 2020. Geochemistry and zircon U-Pb geochronology of Miocene plutons in the Urumieh-Dokhtar magmatic arc, East Tafresh, Central Iran. *Int. Geol. Rev.* 62, 1815–1827. <https://doi.org/10.1080/00206814.2019.1600436>.
- Richards, J.P., Kerrich, R., 2007. Special paper: adakite-like rocks: their diverse origins and questionable role in metallogenesis. *Economic geology* 102 (4), 537–576. <https://doi.org/10.2113/gsecongeo.102.4.537>.
- Richards, J.P., Spell, T., Rameh, E., Raziq, A., Fletcher, T., 2012. High Sr/Y magmas reflect arc maturity, high magmatic water content, and porphyry Cu ± Mo ± Au potential: examples from the Tethyan arcs of Central and Eastern Iran and Western Pakistan. *Econ. Geol.* 107, 295–332. <https://doi.org/10.2113/econgeo.107.2.295>.
- Rossetti, F., Nasrabady, M., Theye, T., Gerdes, A., Monié, P., Lucci, F., Vignaroli, G., 2014. Adakite differentiation and emplacement in a subduction channel: The late Paleocene Sabzevar magmatism (NE Iran). *GSA Bull.* 126, 317–343. <https://doi.org/10.1130/B30913.1>.
- Sahandi, R., Soheili, M., Sadeghi, M., Delavar, T., Jafari Rad, A., 2014. *Compiled Geological Map of Iran, Scale 1:1.000.000, Digitally Published by the Geological Survey of Iran*.
- Sajona, F.G., Maury, R.C., Bellon, H., Cotten, J., Defant, M.J., Pubellier, M., 1993. Initiation of subduction and the generation of slab melts in western and eastern Mindanao, Philippines. *Geology* 21, 1007–1010. [https://doi.org/10.1130/0091-7613\(1993\)021<1007:IOSATG>2.3.CO;2](https://doi.org/10.1130/0091-7613(1993)021<1007:IOSATG>2.3.CO;2).
- Salari, G., Lustrino, M., Ghorbani, M.R., Agostini, S., Fedele, L., 2021. Petrological characterization of the Cenozoic igneous rocks of the Tafresh area, central Urumieh-Dokhtar Magmatic Arc (Iran). *Period. Mineral.* 90, 59–83. <https://doi.org/10.13133/2239-1002/16620>.
- Sepidbar, F., Moghadam, H.S., Li, C., Stern, R.J., Jiantang, P., Vesali, Y., 2020. Cadomian magmatic rocks from Zarand (SE Iran) formed in a Retro-Arc Basin. *Lithos* 366–367, 105569. <https://doi.org/10.1016/j.lithos.2020.105569>.
- Shafaii Moghadam, H., Li, Q.L., Li, X.H., Stern, R.J., Levresse, G., Santos, J.F., Lopez Martinez, M., Ducea, M.N., Ghorbani, G., Hassannezhad, A., 2020. Neotethyan subduction ignited the Iran Arc and backarc differently. *J. Geophys. Res. Solid Earth* 125, 1–30. <https://doi.org/10.1029/2019JB018460>.
- Shafiei, B., Haschke, M., Shahabpour, J., 2009. Recycling of orogenic arc crust triggers porphyry Cu mineralization in Kerman Cenozoic arc rocks, southeastern Iran. *Mineral. Deposita* 44, 265–283. <https://doi.org/10.1007/s00126-008-0216-0>.
- Shahbazi, H., Taheri Maghami, Y., Azizi, H., Asahara, Y., Siebel, W., Maanijou, M., Rezaei, A., 2021. Zircon U-Pb ages and petrogenesis of late Miocene adakitic rocks from the Sari Gunay gold deposit, NW Iran. *Geol. Mag.* 158, 1733–1755. <https://doi.org/10.1017/S0016756821000297>.
- Sisson, T.W., Ratajeski, K., Hankins, W.B., Glazner, A.F., 2005. Voluminous granitic magmas from common basaltic sources. *Contrib. Mineral. Petrol.* 148, 635–661. <https://doi.org/10.1007/s00410-004-0632-9>.
- Sun, S.S., McDonough, W.F., 1989. Chemical and isotopic systematics of oceanic basalts: Implications for mantle composition and processes. *Geol. Soc. Spec. Publ.* 42, 313–345. <https://doi.org/10.1144/GSL.SP.1989.042.01.19>.
- Torkian, A., Furman, T., Salehi, N., Veloski, K., 2019. Petrogenesis of adakites from the Sheyda volcano, NW Iran. *J. Afr. Earth Sci.* 150, 194–204. <https://doi.org/10.1016/j.jafrearsci.2018.11.014>.
- van der Boon, A., 2017. *From Peri-Tethys to Paratethys: Basin Restriction and Anoxia in Central Eurasia Linked to Volcanic Belts in Iran*. Utrecht University. PhD thesis.
- van der Boon, A., Kuiper, K.F., Villa, G., Renema, W., Meijers, M.J.M., Langereis, C.G., Aliyeva, E., Krijgsman, W., 2017. Onset of Maikop sedimentation and cessation of Eocene arc volcanism in the Talys Mountains, Azerbaijan. *Geol. Soc. Lond. Spec. Publ.* 428, 145–169. <https://doi.org/10.1144/sp428.3>.
- van der Boon, A., Kuiper, K., van der Ploeg, R., Cramwinckel, M., Honarmand, M., Sluijs, A., Krijgsman, W., 2021. Exploring a link between the middle eocene climatic optimum and neotethys continental arc flare-up. *Clim. Past* 17, 229–239. <https://doi.org/10.5194/cp-2020-48>.
- Verdel, C., Wernicke, B.P., Hassanzadeh, J., Guest, B., 2011. A Paleogene extensional arc flare-up in Iran. *Tectonics* 30, 1–20. <https://doi.org/10.1029/2010TC002809>.
- Wood, D.A., 1980. The application of a Th/HfTa diagram to problems of tectonomagmatic classification and to establishing the nature of crustal contamination of basaltic lavas of the British Tertiary Volcanic Province. *Earth Planet. Sci. Lett.* 50, 11–30. [https://doi.org/10.1016/0012-821X\(80\)90116-8](https://doi.org/10.1016/0012-821X(80)90116-8).
- Yeganehfar, H., Ghorbani, M.R., Shinjo, R., Ghaderi, M., 2013. Magmatic and geodynamic evolution of Urumieh–Dokhtar basic volcanism, Central Iran: Major, trace element, isotopic, and geochronologic implications. *Int. Geol. Rev.* 55, 767–786. <https://doi.org/10.1080/00206814.2012.752554>.
- Yogodzinski, G.M., Kelemen, P.B., 1998. Slab melting in the Aleutians: Implications of an ion probe study of clinopyroxene in primitive adakite and basalt. *Earth Planet. Sci. Lett.* 158, 53–65. [https://doi.org/10.1016/S0012-821X\(98\)00041-7](https://doi.org/10.1016/S0012-821X(98)00041-7).
- Yousefi, F., Sadeghian, M., Wanhainen, C., Ghasemi, H., Frei, D., 2017. Geochemistry, petrogenesis and tectonic setting of middle Eocene hypabyssal rocks of the Torud–Ahmad Abad magmatic belt: An implication for evolution of the northern branch of Neo-Tethys Ocean in Iran. *J. Geochem. Explor.* 178, 1–15. <https://doi.org/10.1016/j.gexplo.2017.03.008>.
- Zindler, A., Hart, S., 1986. Chemical geodynamics. *Annu. Rev. Earth Planet. Sci.* 14, 493–571. <https://doi.org/10.1146/annurev.ea.14.050186.002425>.